

Intrinsic ecological dynamics drive biodiversity turnover in model metacommunities

Jacob D. O'Sullivan ¹✉, J. Christopher D. Terry ¹ & Axel G. Rossberg¹

Turnover of species composition through time is frequently observed in ecosystems. It is often interpreted as indicating the impact of changes in the environment. Continuous turnover due solely to ecological dynamics—species interactions and dispersal—is also known to be theoretically possible; however the prevalence of such autonomous turnover in natural communities remains unclear. Here we demonstrate that observed patterns of compositional turnover and other important macroecological phenomena can be reproduced in large spatially explicit model ecosystems, without external forcing such as environmental change or the invasion of new species into the model. We find that autonomous turnover is triggered by the onset of ecological structural instability—the mechanism that also limits local biodiversity. These results imply that the potential role of autonomous turnover as a widespread and important natural process is underappreciated, challenging assumptions implicit in many observation and management tools. Quantifying the baseline level of compositional change would greatly improve ecological status assessments.

¹School of Biological and Chemical Sciences, Queen Mary University of London, London, UK. ✉email: j.osullivan@qmul.ac.uk

Change in species composition observed in a single location through time, called community turnover, is observed in all natural ecosystems. Potential drivers of such biotic change include changes in the abiotic environment, random demographic fluctuations (referred to as community drift) and population dynamics driven by ecological interactions and dispersal. Analysis of community time series suggests communities turn over at a faster rate than can be explained by random drift^{1,2}. Climate change and other anthropogenic pressures are known to contribute to community turnover^{3–7} and there is evidence to suggest that turnover is accelerating in some biomes⁸.

Ecological assessments, projections and mitigation strategies are therefore commonly designed around the assumption that communities turn over predominantly in response environmental change and direct anthropogenic pressures⁹. The extent to which processes intrinsic to ecosystems contribute to turnover, however, remains poorly understood¹⁰. Understanding the expected amount of temporal turnover due to such intrinsic processes is of vital importance if ecological change is to be accurately interpreted⁷. If strong temporal community turnover were a natural phenomenon that can arise independently of changes in the abiotic environment, then observed shifts in the composition of ecological communities would not on their own demonstrate external pressures.

In theoretical models of ecological communities population abundances do not necessarily arrive at fixed points. Instead, such systems can manifest persistent dynamics which we refer to here as ‘autonomous’ since they do not depend on variation in the external environment or other extrinsic drivers. When these population fluctuations are strong, changes in the abundances of species can be dramatic and even drive species locally extinct; if an excluded species retains occupancy in adjacent patches¹¹, it may re-colonise at some future time. We refer to as ‘autonomous turnover’ local compositional changes involving colonisation-extinction processes or significant restructuring of relative abundances, driven by such autonomous population dynamics.

Limited availability of historical turnover data before the onset of widespread anthropogenic impacts poses considerable challenges when trying to establish the natural baseline of turnover. Nevertheless, broad consistency amongst the species-time-area relationships observed in extant assemblages^{12,13} points to a consistency in the dominant underlying biological process. It is reasonable to expect, therefore, that the drivers of such spatio-temporal turnover can be probed using theoretical models.

Previous theoretical^{11,14–17} and experimental studies¹⁸ have shown how competitive ecological communities (for specific network structures or parameter combinations) can generate any type of dynamical behaviour, including persistent chaotic cycles. Likewise, antagonistic interactions between predator and prey species have been shown in both theory and experiment to lead to persistent population oscillations in the absence of external variation^{19,20}. However, these cyclic processes are different from, and have not usually been associated with, empirical observations of acyclic, directional compositional turnover^{1,2}. An important distinction between these processes lies in the role of space. While cyclic forms of community dynamics can lead to characteristic spatial structures^{17,18,21}, cyclic dynamics do not in principle require space^{19,20}. Acyclic turnover, on the other hand, manifestly involves colonisation by species from surrounding patches and therefore explicitly requires that a community is embedded in a spatially structured ecological neighbourhood.

Here we ask: can community dynamics enabled by spatial structure account for the observed macroecological patterns in compositional turnover? We address this question drawing on recent advances in the theory of spatially extended ecological communities, so called “metacommunities”²², using a

population-dynamical simulation model with explicit spatial and environmental structure²³ that has been shown to reproduce fundamental *spatial* biodiversity patterns. As previously shown, such metacommunity models can exhibit a phenomenon called “ecological structural instability”²⁴, as a result of which species richness at both local and regional scales is intrinsically regulated²³. The structural stability of a system refers to its capacity to sustain changes in parameters without undergoing qualitative changes in dynamical behaviour²⁵. As such, ecological structural stability is taken to describe in particular the capacity of a community to *persist* in the face of small biotic or abiotic perturbations^{24,26–30}. Empirical observation of many of the emergent phenomena associated with ecological structural instability provides compelling indirect evidence for the prevalence of structural instability in nature^{23,31}. Our understanding of the impact of structurally unstable diversity regulation on temporal community-level properties, however, remains incomplete³². Here we build upon earlier work by exploring the spatio-temporal patterns that emerge in metacommunity models. We find that, when expanding the spatial and taxonomic scale of simulations beyond those studied previously, metacommunities manifest autonomous compositional turnover which can be substantial and, in the case of large models, acyclic. This turnover is best understood as continuous fluctuations of community state around heteroclinic networks characterised by multiple unstable equilibria. Crucially, the macroecology of these heteroclinic networks matches known empirical patterns.

Results and discussion

Metacommunity model and asymptotic community assembly.

We built a large set of model metacommunities (detailed in full in “Methods”) describing competitive dynamics within a single guild of species across a landscape. Each metacommunity consisted of a set of patches, or local communities, randomly placed in a square arena and linked by a spatial network. The dynamics of each population are governed by three processes: inter- and intraspecific interactions, heterogeneous responses to the environment and dispersal between adjacent patches (Fig. 1). Competition coefficients between species are drawn at random and the population dynamics within each patch are described by a Lotka-Volterra competition model. We control the level of environmental heterogeneity across the network directly by generating an intrinsic growth rate for each species at each patch from a random, spatially correlated distribution. To ensure any turnover is purely autonomous, we keep the environment fixed throughout simulations. Dispersal between neighbouring patches declines exponentially with distance between sites. This formulation allows precise and independent control of key properties of the metacommunity—the number of patches, the characteristic dispersal length and the heterogeneity of the environment.

To populate the model metacommunities, we iteratively introduced species with randomly generated intrinsic growth rates and interspecific interaction coefficients. Between successive regional invasions we simulated the model dynamics, and removed any species whose abundance fell below a threshold across the whole network. Through this assembly process and the eventual onset of ecological structural instability, both average local diversity, the number of species coexisting in a given patch, and regional diversity, the total number of species in the metacommunity, eventually saturate and then fluctuate around an equilibrium value—any introduction of a new species then leads on average to the extinction of one other species (Supplementary Fig. 1). In these intrinsically regulated metacommunities we then studied the phenomenology of autonomous community turnover *in the absence of regional invasions or abiotic change*.

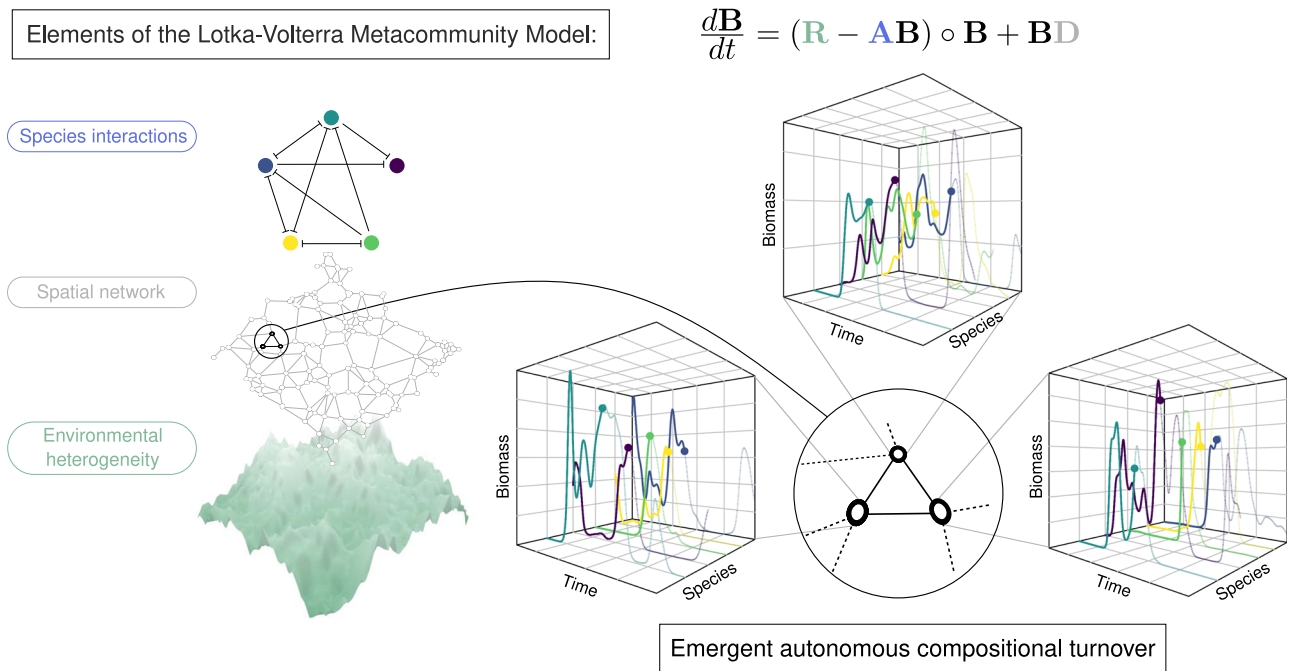


Fig. 1 Elements of the Lotka-Volterra metacommunity model and the emergence of autonomous population dynamics. Environmental heterogeneity, represented by the intrinsic growth rate matrix \mathbf{R} , is modelled using a spatially autocorrelated Gaussian random field. A random spatial network, represented by the dispersal matrix \mathbf{D} , defines the spatial connectivity of the landscape. The network of species interactions, represented by the competitive overlap matrix \mathbf{A} , is modelled by sampling competition coefficients at random (perpendicular bars indicate recipients of a deleterious competitive impact). The resulting dynamics of local population biomasses, given by the colour-coded equation, are numerically simulated. The Hadamard product ‘ \circ ’ represents element-wise matrix multiplication. For large metacommunities, local populations exhibit persistent dynamics despite the absence of external drivers. In the 3D boxes, typical simulated biomass dynamics of dominating species are plotted on linear axes over 2500 unit times. The graphs illustrate the complexity of the autonomous dynamics and the propensity for compositional change (local extinction and colonisation).

In our metacommunity model, local community dynamics and therefore local limits on species richness depend on a combination of biotic and abiotic filtering (non-uniform responses of species to local conditions)^{33–35} and immigration from adjacent patches, generating so called mass effects in the local community^{36–38}. Biotic filtering via interspecific competition is encoded in the interaction coefficients A_{ij} , while abiotic filtering occurs via the spatial variation of intrinsic growth rates R_{ix} . For simplicity, and since predator-prey dynamics are known to generate oscillations³⁹ through mechanisms distinct from those we report here, we restrict our analysis to competitive communities for which all ecological interactions are antagonistic. The off-diagonal elements of the interaction matrix \mathbf{A} describe how one species i affects another species j . These are sampled independently from a discrete distribution, such that the interaction strength A_{ij} is set to a constant value in the range 0 to 1 (in most cases 0.5) with fixed probability (connectance, in most cases 0.5) and otherwise set to zero. Intraspecific competition coefficients A_{ii} are set to 1 for all species. This discrete distribution of the interaction terms was chosen for its relative efficiency. In the Supplementary discussion (and Supplementary Fig. 2) we show that outcomes remain unaffected when more complex distributions are modelled. Intrinsic growth rates R_{ix} are sampled from spatially correlated normal distributions with mean 1, autocorrelation length ϕ and variance σ^2 (Supplementary Fig. 3).

Dispersal is modelled via a spatial connectivity matrix with elements D_{xy} . The topology of the model metacommunity, expressed through \mathbf{D} , is generated by sampling the spatial coordinates of N patches from a uniform distribution $\mathcal{U}(0, \sqrt{N}) \times \mathcal{U}(0, \sqrt{N})$, i.e., an area of size N . Thus, under variation of the number of patches, the inter-patch distances

remain fixed on average. Spatial connectivity is defined by linking these patches through a Gabriel graph⁴⁰, a planar graph generated by an algorithm that, on average, links each local community to four close neighbours⁴¹. Avoidance of direct long-distance dispersal and the sparsity of the resulting dispersal matrix permit the use of efficient numerical methods. The exponential dispersal kernel defining D_{xy} is tuned by the dispersal length ℓ , which is fixed for all species.

The dynamics of local population biomasses $B_{ix} = B_{ix}(t)$ are modelled using a system of spatially coupled Lotka-Volterra (LV) equations that, in matrix notation, takes the form²³

$$\frac{d\mathbf{B}}{dt} = \mathbf{B} \circ (\mathbf{R} - \mathbf{A}\mathbf{B}) + \mathbf{B}\mathbf{D}, \tag{1}$$

with \circ denoting element-wise multiplication. Hereafter this formalism is referred to as the Lotka-Volterra Metacommunity Model (LVMCM). Further technical details are provided in Methods and the Supplementary Discussion.

In order to numerically probe the impacts of ℓ , ϕ and σ^2 on the emergent temporal dynamics, we initially fixed $N = 64$ and varied each parameter through multiple orders of magnitude (Supplementary Fig. 4). In order to obtain a full characterisation of autonomous turnover in the computationally accessible spatial range ($N \leq 256$), we then selected a parameter combination found to generate substantial fluctuations for further analysis. Thereafter we assembled metacommunities of 8–256 patches (Fig. 2a) until regional diversity limits were reached (with tenfold replication) and generated community time series of 10^4 unit times from which the phenomenology of autonomous turnover could be explored in detail. We found no evidence to suggest that the phenomenology described below depends on this specific parameter combination. While future results may confirm or

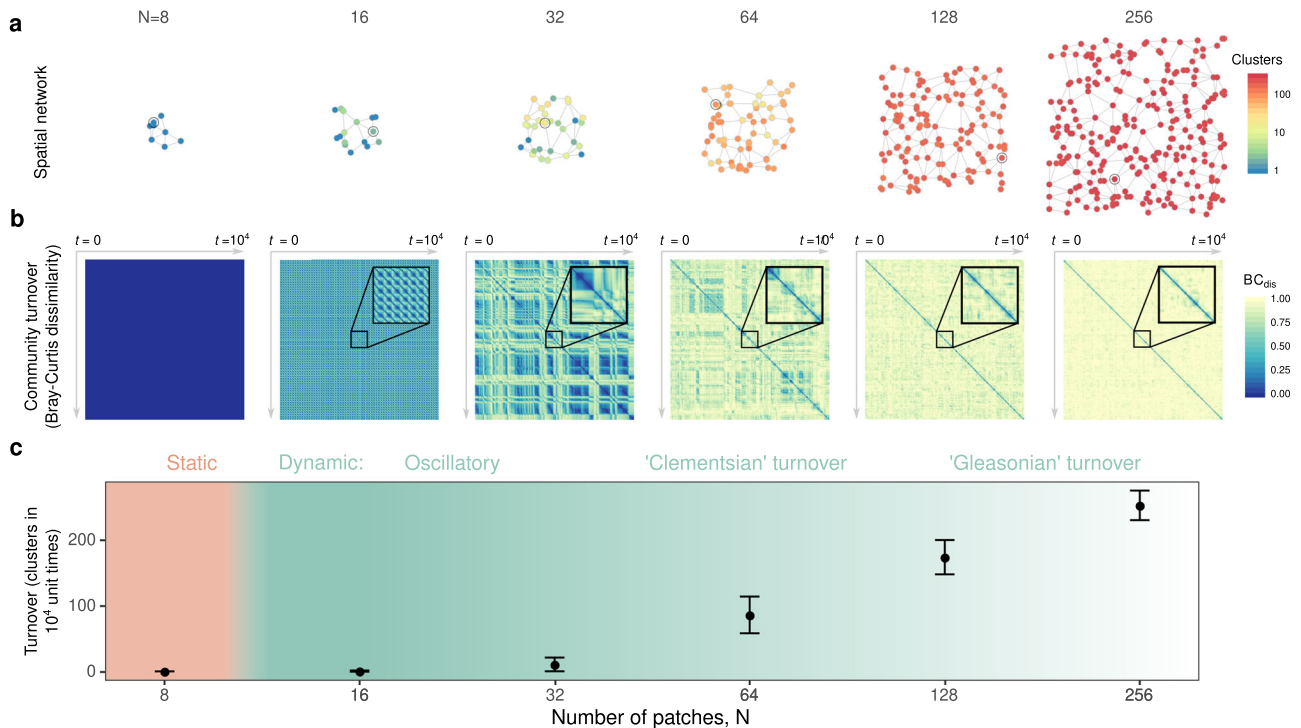


Fig. 2 Autonomous turnover in model metacommunities. **a** Typical model metacommunities: a spatial network with N nodes representing local communities (or patches) and edges, channels of dispersal. Patch colour represents the number of clusters in local community state space detected over 10^4 unit times t using hierarchical clustering of the Bray-Curtis (BC) dissimilarity matrix, Supplementary Fig. 6. **b** Colour coded matrices of pairwise temporal BC dissimilarity corresponding to the circled patches in (a). Insets represent 10^2 unit times. For small networks ($N = 8$) local compositions converge to static fixed points. As metacommunity extent increases, however, persistent dynamics emerge. Initially this autonomous turnover is oscillatory in nature with communities fluctuating between small numbers of states which can be grouped into clusters ($16 \leq N \leq 32$). Intermediate metacommunities ($32 \leq N \leq 64$) manifest “Clementsian” temporal turnover, characterised by sharp transitions in composition, implying species turn over in cohorts. Large metacommunities ($N \geq 128$) turn over continuously, implying “Gleasonian” assembly dynamics in which species’ temporal occupancies are independent. **c** The mean number of local compositional clusters detected for metacommunities of various numbers of patches N (error bars represent standard deviation across all replicated simulations). While the transition from static to dynamic community composition at the local scale is sharp (see text), non-uniform turnover *within* metacommunities (a) blurs the transition at the regional scale. $A_{ij} = 0.5$ with probability 0.5, $\phi = 10$, $\sigma^2 = 0.01$, $\ell = 0.5$.

refute this, autonomous turnover arises over a wide range of parameters (Supplementary Fig. 4) and as such the phenomenon is robust.

Autonomous turnover in model metacommunities. For small ($N \leq 8$) metacommunities assembled to regional diversity limits, populations attain equilibria, i.e., converge to fixed points, implying the absence of autonomous turnover²³. With increasing metacommunity size N , however, we observe the emergence of persistent population dynamics (Supplementary Fig. 5 and external video) that can produce substantial turnover in local community composition. This autonomous turnover can be represented through Bray-Curtis⁴² (BC) dissimilarity matrices comparing local community composition through time (Fig. 2b), and quantified by the number of compositional clusters detected in such matrices using hierarchical cluster analysis (Fig. 2a, c).

At intermediate spatial scales (Fig. 2, $16 \leq N \leq 32$) we often find oscillatory dynamics, which can be perfectly periodic or slightly irregular. With increasing oscillation amplitude, these lead to persistent turnover dynamics where local communities repeatedly transition between a small number of distinct compositional clusters (represented in Fig. 2 by stripes of high pairwise BC dissimilarity spanning large temporal ranges). At even larger scales ($N \geq 64$) this compositional coherence begins to break down, and for very large metacommunities ($N \geq 128$) autonomous dynamics drive continuous acyclic change in community composition. The number of compositional clusters

detected over time typically varies within a given metacommunity (Fig. 2a node colour), however we find a clear increase in the average number of compositional clusters, i.e., an increase in turnover, with increasing total metacommunity size (Fig. 2c).

Metacommunities in which the boundaries of species ranges along environmental gradients are clumped are termed *Clementsian*, while those for which range limits are independently distributed are referred to as *Gleasonian*⁴³. We consider the block structure of the temporal dissimilarity matrix at intermediate N to represent a form of Clementsian temporal turnover, characterised by sudden significant shifts in community composition. Metacommunity models similar to ours have been found to generate such patterns along spatial gradients⁴⁴, potentially via an analogous mechanism⁴⁵. Large, diverse model metacommunities manifest Gleasonian temporal turnover. In such cases, species colonisations and extirpations are largely independent and temporal occupancies predominantly uncorrelated, such that compositional change is continuous, rarely, if ever, reverting to the same state.

Mechanistic explanation of autonomous turnover. Surprisingly, the onset and increasing complexity of autonomous turnover as system size N increases (Fig. 2) can be understood as a consequence of local community dynamics alone. To explain this, we first recall relevant theoretical results for isolated LV communities. Then we demonstrate that, in presence of weak propagule pressure, these results imply local community turnover dynamics,

controlled by the richness of potential invaders, that closely mirror the dependence on system size seen in full LV metacommunities.

Application of methods from statistical mechanics to models of large isolated LV communities with random interactions revealed that such models exhibit qualitatively distinct phases^{46–48}. If the number of modelled species, S , interpreted as species pool size, lies below some threshold value determined by the distribution of interaction strengths (Supplementary Fig. 7), these models exhibit a unique linearly stable equilibrium (Unique Fixed Point phase, UFP). Some species may go extinct, but the majority persists⁴⁸. When pool size S exceeds this threshold, there appear to be no more linearly stable equilibrium configurations. Any community formed by a selection from the S species is either unfeasible (there is no equilibrium with all species present), intrinsically linearly unstable, or invadable by at least one of the excluded species. This has been called the multiple attractor (MA) phase⁴⁷. However, the implied notion that this part of the phase space is in fact characterised by multiple stable equilibria may be incorrect.

Population dynamical models with many species have been shown to easily exhibit attractors called stable heteroclinic networks⁴⁹, which are characterised by dynamics in which the system bounces around between several unstable equilibria, each corresponding to a different composition of the extant community, implying indefinite, autonomous community turnover (Fig. 3, red line). As these attractors are approached, models exhibit increasingly long intermittent phases of slow dynamics, which, when numerically simulated, can give the impression that the system eventually reaches one of several ‘stable’ equilibria, suggesting that turnover comes to a halt. We demonstrate in the Supplementary discussion that the MA phase of isolated LV models is in fact characterised by such stable heteroclinic networks (Supplementary Figs. 8 and 9). Note, we retain the MA terminology here because the underlying complete

heteroclinic networks, interpreted as a directed graph^{50,51} (Fig. 3, inset), might have multiple components that are mutually unreachable through dynamic transitions⁵², each representing a different attractor.

If one now adds to such isolated LV models terms representing weak propagule pressure for all S species (Supplementary Eq. (2)), dynamically equivalent to mass effects occurring in the full metacommunity model (Eq. (1)), then none of the S species can entirely go extinct. The weak influx of biomass drives community states away from the unstable equilibria representing coexistence of subsets of the S species and the heteroclinic network connecting them (blue line in Fig. 3). Typically, system dynamics then still follow trajectories closely tracking the original heteroclinic networks (Fig. 3), but now without requiring boundless time to transition from the vicinity of one equilibrium to the next.

The nature and complexity of the resulting population dynamics depend on the size and complexity of the underlying heteroclinic network, and both increase with pool size S . In simulations (Supplementary Fig. 10) we find that, as S increases, LV models with weak propagule pressure pass through the same sequence of states as we documented for LVMCM metacommunities in Fig. 2: equilibria, oscillatory population dynamics, Clementsian and finally Gleasonian temporal turnover.

Above we introduced the number of clusters detected in Bray-Curtis dissimilarity matrices of fixed time series length as a means of quantifying the approximate number of equilibria visited during local community turnover. As shown in Fig. 4a, b, this number increases in LV models with S in a manner strikingly similar to its increase in the LVMCM with the number of species present in the ecological neighbourhood of a given patch. Thus, dynamics within a patch are controlled not by N directly but rather by neighbourhood species richness. For a given neighbourhood, species richness depends on the number of connected patches, the total area and therefore total abiotic heterogeneity encompassed, and the connectivity, all of which can vary substantially within a metacommunity of a given size N . As illustrated in Fig. 4b, there is a tendency for neighbourhood richness to be larger in larger metacommunities, leading indirectly to the dependence of metacommunity dynamics on N seen in Fig. 2.

There is thus a close correspondence between dynamically isolated LV models and LVMCM metacommunities, in the sequence of dynamic states as propagule richness increases and in the resulting complexity of dynamics quantified by counting compositional clusters. This suggests that underlying heteroclinic networks, which are revealed by adding propagule pressure in isolated communities, explain the complex dynamics seen in LVMCM metacommunities.

For the isolated LV community, the threshold beyond which autonomous turnover is detected (>1 compositional cluster) occurs at a pools size of around $S = 35$ species, consistent with the theoretical prediction⁴⁷ of the transition between the UFP and MA phases (Supplementary Discussion). Close inspection of this threshold reveals an important and hitherto unreported relationship between the transition into the MA phase and local ecological limits set by the onset of ecological structural instability, which is known to regulate species richness in LV systems subject to external invasion pressure^{23,24}: in the Supplementary Discussion we show that the boundary between the UFP and MA phases⁴⁷ coincides precisely with the onset of structural instability²⁴ (Supplementary Eqs. (3)–(9)).

For LVMCM metacommunities, this relationship (demonstrated analytically in the Supplementary Discussion) is numerically confirmed in Fig. 5. During assembly, local species richness increases until it reaches the limit imposed by local structural

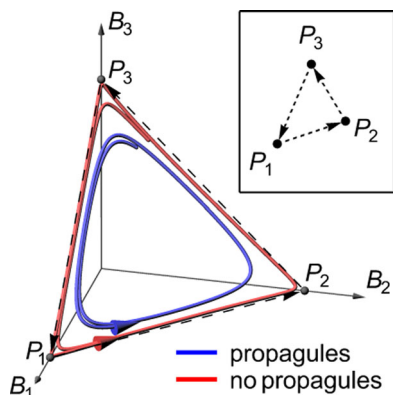


Fig. 3 Approximate heteroclinic networks underlie autonomous community turnover.

The main panel shows two trajectories in the state space of a community of three hypothetical species (population biomasses B_1 , B_2 , B_3) that are in non-hierarchical competition with each other, such that no species can competitively exclude both others (a ‘rock-paper-scissors game’¹⁷). Without propagule pressure, the system has three unstable equilibrium points (P_1 , P_2 , P_3) and cycles between these (red curve), coming increasingly close to the equilibria and spending ever more time in the vicinity of each. The corresponding attractor is called a heteroclinic cycle (dashed arrows). Under weak extrinsic propagule pressure (blue curve), the three equilibria and the heteroclinic cycle disappear, yet the system closely tracks the original cycle in state space. Such a cycle can be represented as a graph linking the dynamically connected equilibria (inset). With more interacting species, these graphs can become complex ‘heteroclinic networks’^{49–51} with trajectories representing complex sequences of species composition during autonomous community turnover.

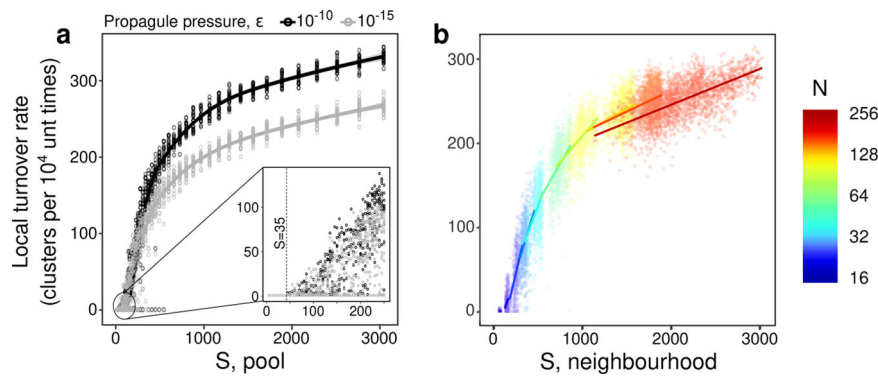


Fig. 4 Ecological mass effects drive autonomous turnover. **a** The number of compositional clusters detected, plotted against the size of the pool of potential invaders S for an isolated LV community using a propagule pressure ϵ of 10^{-10} and 10^{-15} , fit by a generalised additive model⁸⁷. For $S < 35$ a single cluster is detected. For $S \geq 35$ autonomous turnover occurs (≥ 1 compositional clusters) with the transition indicated by the dashed line (inset). **b** Qualitatively identical behaviour was observed for model metacommunities in which “propagule pressure” arises due to ecological mass effects from the local neighbourhood. Each point represents a single patch. Lines in **(b)** are standard linear regressions. The good alignment of subsequent fits demonstrates that neighbourhood diversity is the dominating predictor of cluster number, rather than patch number N . $A_{ij} = 0.5$ with probability 0.5, $\phi = 10$, $\sigma^2 = 0.01$, $\ell = 0.5$.

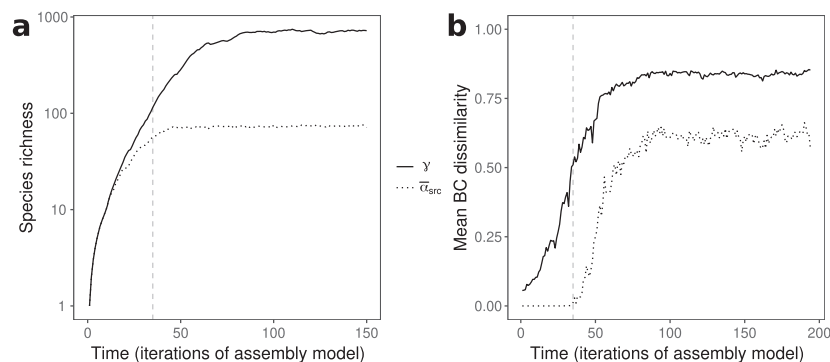


Fig. 5 The emergence of temporal turnover during metacommunity assembly. **a** Local species richness, defined by reference to source populations only ($\bar{\alpha}_{src}$, grey) and regional diversity (γ black) for a single metacommunity of $N = 32$ coupled communities during iterative regional invasion of random species. We quantify local source diversity $\bar{\alpha}_{src}$ as the metacommunity average of the number α_{src} of non-zero equilibrium populations persisting when immigration is switched off (off-diagonal elements of \mathbf{D} set to zero), since this is the component of a local community subject to strict ecological limits to biodiversity. Note the log scale chosen for easy comparison of local and regional species richness. **b** Increases in regional diversity beyond local limits arise via corresponding increases in spatial turnover ($\bar{\beta}_s$, black). Autonomous temporal turnover ($\bar{\beta}_t$, grey) sets in (crosses a threshold mean Bray Curtis (BC) dissimilarity of 10^{-2}) precisely when average local species richness $\bar{\alpha}_{src}$ has reached its limit, reflecting the equivalence of the transition to the MA phase space and the onset of local structural instability. In both panels, the dashed line marks the point at which autonomous temporal turnover was first detected. $A_{ij} = 0.3$ with probability 0.3, $\phi = 10$, $\sigma^2 = 0.01$, $\ell = 0.5$. Both spatial and temporal turnover computed as the mean BC dissimilarity. In each iteration of the assembly model (regional invasion event), $0.15 + 1$ species were introduced. Dynamics were simulated for 2×10^4 unit times, with the second 10^4 unit times analysed for autonomous turnover, and a total of 10^4 invasions were modelled.

instability. Further assembly occurs via the “regionalisation” of the biota⁵³—a collapse in average range sizes²³ and associated increase in spatial beta diversity—until regional diversity limits are reached²³. The emergence of autonomous turnover coincides with the onset of species saturation at the local scale. Autonomous turnover can therefore serve as an indirect indication of intrinsic biodiversity regulation via local structural instability in complex communities.

Thus, we have shown that propagule pressure perturbs local communities away from unstable equilibria and drives compositional change. In order to invade, however, species need to be capable of passing through biotic and abiotic filters^{33–35}. We would expect, therefore, that turnover would be suppressed in highly heterogeneous or poorly connected environments where mass effects are weak. Indeed, by manipulating the autocorrelation length ϕ and variance σ^2 of the abiotic filter represented by the matrix \mathbf{R} and the characteristic dispersal length ℓ , we observe a sharp drop-off in temporal turnover in parameter regimes that

maximise between-patch community dissimilarity (short environmental correlation or dispersal lengths, Supplementary Fig. 11). Thus, we conclude that it is not species richness or spatial dissimilarity per se that best predict temporal turnover, but the size of the pool of species with positive invasion fitness, i.e., those not repelled by the combined effects of biotic and abiotic filters.

The macroecology of autonomous turnover. We find good correspondence between temporal and spatio-temporal biodiversity patterns emerging in model metacommunities in the absence of external abiotic change and in empirical data (Fig. 6), with quantitative characteristics lying within the ranges observed in natural ecosystems.

Temporal occupancy. The proportion of time in which species occupy a community tends to have a bi-modal empirical distribution^{54–56} (Fig. 6a). The distribution we found in simulations (Fig. 6e) closely matches the empirical pattern.

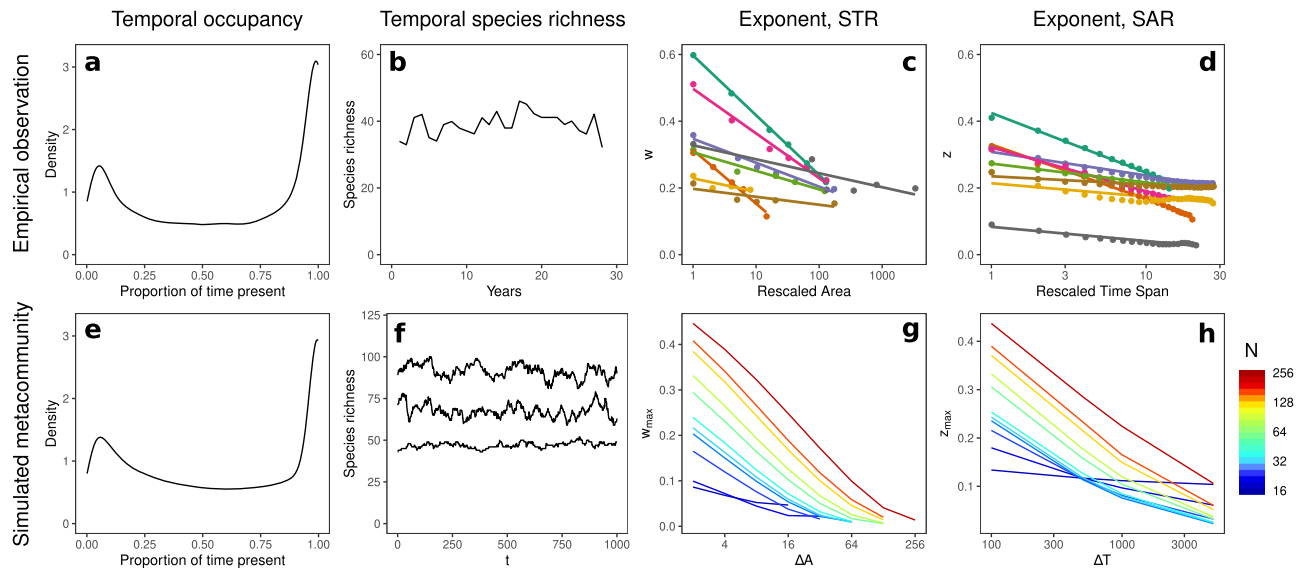


Fig. 6 Macroecological signatures of autonomous compositional change. A bimodal distribution in temporal occupancy observed in North American birds⁵⁴ (a) and in simulations (e $N = 64$, $\phi = 5$, $\sigma^2 = 0.01$, $\ell = 0.5$). Intrinsically regulated species richness observed in estuarine fish species⁵⁹ (b) and in simulations (f $N = 64$, $\phi = 5$, $\sigma^2 = 0.01$, $\ell = 0.5$, 1000 unit times t). The decreasing slopes of the STR with increasing sample area¹² (c), and the SAR with increasing sample duration¹² (d) for various communities and in simulations (g and h $N = 256$, $\phi = 10$, $\sigma^2 = 0.01$, $\ell = 0.5$, spatial window ΔA , temporal window ΔT). In (c) and (d) we have rescaled the sample area/duration by the smallest/shortest reported value and coloured by community (see original study for details). In (g) and (h) we study the STAR in metacommunities of various size N , represented by colour. Limited spatio-temporal turnover in the smallest metacommunities (blue colours) greatly reduces the exponents of the STAR relative to large metacommunities (red colours). $A_{ij} = 0.5$ with probability 0.5 in all cases.

Community structure. Temporal turnover has been posited to play a stabilising role in the maintenance of community structure^{57,58}. In an estuarine fish community⁵⁹, for example, species richness (Fig. 6b) and the distribution of abundances were remarkably robust despite changes in population biomasses by multiple orders of magnitude. In model metacommunities with autonomous turnover we found, likewise, that local species richness exhibited only small fluctuations around the steady-state mean (Fig. 6f, three random local communities shown) and that the macroscopic structure of the community was largely time invariant (Supplementary Fig. 12). In the light of our results, we propose the absence of temporal change in community properties such as richness or the abundance distribution despite potentially large fluctuations in population abundances⁵⁹ as indicative of autonomous compositional turnover.

The species-time-area-relation, STAR. The species-time-relation (STR), typically fit by a power law of the form $S \propto T^w$ ^{12,60,61}, describes how observed species richness increases with observation time T . The exponent w of the STR has been found to be consistent across taxonomic groups and ecosystems^{12,13,62}, indicative of some general population dynamical mechanism. However, the exponent of the STR decreases with increasing sampling area¹², and the exponent of the empirical Species Area Relation (SAR) ($S \propto A^z$) consistently decreases with increasing sampling duration¹² (Fig. 6c, d). We tested for these patterns in a large simulated metacommunity with $N = 256$ patches by computing the species-time-area-relation (STAR) for nested subdomains and variable temporal sampling windows (see “Methods”). We observed exponents of the nested SAR in the range $z = 0.02$ – 0.44 and for the STR a range $w = 0.01$ – 0.44 (Supplementary Fig. 13). We also found a clear decrease in the rate of species accumulation in time as a function of sample area and vice-versa (Fig. 6g, h), consistent with the empirical observations. Meta-analyses of these patterns in nature have reported exponents which are remarkably

consistent, with z typically in the range 0.1 – 0.363 , and w typically in the range 0.2 – 0.413 , in both cases largely independent of location or taxonomic group¹³.

Thus, the distribution of temporal occupancy, the time invariance of key macroecological structures and the STAR in our model metacommunities match observed patterns. This evidence suggests that such autonomous dynamics cannot be ruled out as an important driver of temporal compositional change in natural ecosystems.

Turnover rate in simulated metacommunities. How do the turnover rates that we find in our model compare with those observed? Our current analytic understanding of autonomous turnover is insufficient for estimating the rates directly from parameters, but the simulation results provide some indication of the expected order of magnitude, that can be compared with observations. Key for such a comparison is the fact that, because the elements of \mathbf{R} are 1 on average, the time required for an isolated single population to reach carrying capacity is $\mathcal{O}(1)$ unit times. Supplementary Fig. 12b suggests that transitions between community states occur at the scale of around 10–50 unit times. This gives a holistic, rule-of-thumb estimate for the expected rate of autonomous turnover, depending on the typical reproductive rates of the guild of interest. In the case of macroinvertebrates, for example, the time required for populations to saturate in population biomass could be of the order of a month or less. By our rule of thumb, this would mean that autonomous community turnover would occur on a timescale of years. In contrast, for slow growing species like trees, where monoculture stands can take decades to reach maximum population biomass, the predicted timescale for autonomous turnover would be on the order of centuries or more. Indeed, macroinvertebrate communities have been observed switching between community configurations with a period of a few years^{64,65}, while the proportional abundance of tree pollen and tree fern spores fluctuates in rain forest bog

deposits with a period of the order of 10^3 years⁶⁶—suggesting that the predicted autonomous turnover rates are biologically plausible.

Conclusions. Current understanding of the mechanisms driving temporal turnover in ecological communities is predominantly built upon phenomenological studies of observed patterns^{2,67–69} and is unquestionably incomplete^{10,59}. That temporal turnover can be driven by external forces—e.g., seasonal or long term climate change, direct anthropogenic pressures—is indisputable. A vitally important question is, however, how much empirically observed compositional change is actually due to such forcing. Recent landmark analyses of temporal patterns in biodiversity have detected no systematic change in species richness or structure in natural communities, despite rates of compositional turnover greater than predicted by stochastic null models^{1,70–72}. Here we have shown that empirically realistic turnover in model metacommunities can occur via precisely the same mechanism as that responsible for regulating species richness at the local scale. While the processes regulating diversity in natural communities remain insufficiently understood, our theoretical work suggests local structural instability may explain these empirical observations in a unified and parsimonious way. Therefore, we advocate for the application of null models of metacommunity dynamics that account for natural turnover in ecological status assessments and predictions based on ancestral baselines. Future work will involve fitting the model described here to observations by estimating abiotic and biotic parameters from empirical datasets. In the Supplementary Discussion we show how different combinations of parameters lead to different quantitative outcomes (Supplementary Fig. 4), likely representing different types of empirical metacommunities. Understanding where in this parameter space natural systems exist may provide the foundation for a quantitative null model, a baseline expectation of turnover against which observations can be compared.

Our simulations revealed a qualitative transition from “small” metacommunities, where autonomous turnover is absent or minimal, to “large” metacommunities with pronounced autonomous turnover (Fig. 2). The precise location of the transition between these cases depends on details such as dispersal traits, the ecological interaction network, and environmental gradients (Supplementary Fig. 4). Taking, for simplicity, regional species richness as a measure of metacommunity size suggests that both ‘small’ and ‘large’ communities in this sense are realised in nature. In our simulations, the smallest metacommunities sustain 10s of species, while the largest have a regional diversity of the order 10^3 , which is not large comparable to the number of tree species in just 0.25 km² of tropical rainforest (1100–1200 in Borneo and Ecuador⁷³) or of macroinvertebrates in the UK (>32,000⁷⁴). Within the ‘small’ category, where autonomous turnover is absent, we would therefore expect to be, e.g., communities of marine mammals or large fish, where just a few species interact over ranges that can extend across entire climatic niches, implying that the effective number of independent “patches” is small and providing few opportunities for colonisation by species from neighbouring communities. Likely to belong to the ‘large’ category are communities of organisms that occur in high diversity with range sizes that are small compared to climatic niches, such as macroinvertebrates. For these, autonomous turnover of local communities can plausibly be expected based on our findings. Empirically distinguishing between these two cases for different guilds will be an important task for the future.

For metacommunities of intermediate spatial extent, autonomous turnover is characterised by sharp transitions between cohesive states at the local scale. To date, few empirical analyses

have reported such coherence in temporal turnover, perhaps because the taxonomic and temporal resolution required to detect such patterns is not yet widely available. Developments in biomonitoring technologies⁷⁵ are likely to reveal a variety of previously undetected ecological dynamics, however and by combining high resolution temporal sampling and metagenetic analysis of community composition, a recent study demonstrated cohesive but short-lived community cohorts in coastal plankton⁷⁶. Such Clementsian temporal turnover may offer a useful signal of autonomous compositional change in real systems.

Thus, overcoming previous computational limits to the study of complex metacommunities^{11,77}, we have discovered the existence of two distinct phases of metacommunity ecology—one characterised by weak or absent autonomous turnover, the other by continuous compositional change even in the absence of external drivers. By synthesising a wide range of established ecological theory^{11,23,24,47–49}, we have heuristically explained these phases. Our explanation implies that autonomous turnover requires little more than a diverse neighbourhood of potential invaders, a weak immigration pressure, and a complex network of interactions between co-existing species.

Methods

Metacommunity assembly. The dynamics of local population biomasses $B_{ix}(t)$ were modelled using a spatial extension to the multispecies Lotka-Volterra competition model²³:

$$\frac{dB_{ix}}{dt} = B_{ix} \left(R_{ix} - \sum_{j=1}^S A_{ij} B_{jx} \right) - e B_{ix} + \sum_{y \in \mathcal{N}(x)} \frac{e}{k_y} \exp(-d_{xy} \ell^{-1}) B_{iy}. \quad (2)$$

The competitive coupling coefficients A_{ij} for $i \neq j$ were sampled from discrete distributions. Generally, A_{ij} were set to 0.5 with a probability of 0.5 and to 0 otherwise, however, for the simulation shown in Fig. 5, we relaxed the dynamic coupling and instead set A_{ij} to 0.3 with a probability of 0.3. This delayed the onset of local structural instability during metacommunity assembly, making the coincident emergence of local biodiversity regulation and autonomous compositional turnover visually clearer.

Environmental heterogeneity was modelled implicitly through spatial variation in species’ intrinsic growth rates R_{ix} . Specifically, the R_{ix} were sampled independently for each species i from a Gaussian random field⁷⁸ with mean $\mu = 1.0$ and standard deviation σ , generated via spectral decomposition⁷⁹ of the $N \times N$ landscape covariance matrix with elements $\Sigma_{xy} = \exp(-\phi^{-1} d_{xy})$, where d_{xy} denotes the Euclidean distances between patches x and y , and ϕ the autocorrelation length (Supplementary Fig. 3).

The dispersal matrix \mathbf{D} (Eq. (1)) has diagonal elements $D_{xx} = -e$, where e , the fraction of biomass leaving patch x per unit time, was kept fixed at 0.01 for all simulations. For pairs of patches connected by an edge in the spatial network, the immigration terms were modelled as negative exponentials $D_{xy} = e k_y^{-1} \exp(-d_{xy} \ell^{-1})$, controlled by a dispersal length parameter ℓ , thus assuming a propensity for propagules to transition to nearby sites. The normalisation constant k_y divides the biomass departing patches y between all other patches in its local neighbourhood ($\mathcal{N}(y)$), weighted by the ease of reaching each patch i.e., $k_y = \sum_{z \in \mathcal{N}(y)} \exp(-d_{yz} \ell^{-1})$, implying an active dispersal process.

Metacommunities were assembled by iterated regional invasion (Supplementary Fig. 1). In each iteration of the algorithm, $0.05S + 1$ new species were introduced to the metacommunity, with S denoting the current extant species richness. The invaders were tested to ensure positive growth rates at low abundance. This was done by introducing a multiple of $0.05S + 1$ newly generated species into all patches at very low abundance, then simulating for a handful of time steps and testing for increasing biomass trajectories in at least one patch. Of the successful invaders, $0.05S + 1$ were randomly selected and each introduced at 10^{-6} biomass units into the patch in which its growth rate was greatest during testing. After invaders were introduced, metacommunity dynamics were simulated using the SUNDIALS⁸⁰ numerical ODE solver. The time between regional invasions we kept fixed at 500 unit times, and before each new regional invasion the metacommunity was scanned and species with biomass smaller than 10^{-4} biomass units in all patches of the network were considered regionally extinct and removed from the model. The assembly algorithm aims to remove all species whose total biomass declines to zero in the course of the system’s complex dynamics. In rare cases autonomous fluctuations may drive one of the remaining species to very low abundance in all patches, however the majority retain local biomass above the detection threshold in at least one patch at all times.

To assemble models of sufficient spatial extent and species richness, we developed a parallel implementation of the assembly model that makes use of the

algorithmic domain decomposition method⁸¹ for the population-dynamical simulations. This involves decomposing the metacommunity into spatial subdomains of equal numbers of patches, each of which is simulated by a unique parallel process (CPU), with boundary states regularly broadcast between processes. The code was run on the Apocrita high-performance cluster at Queen Mary, University of London⁸². This permitted assembly of saturated metacommunities of up to $N = 256$ patches harbouring $S \sim 3000$ species, thus breaking through frequently lamented computational limits^{11,77} on the numerical study of metacommunities.

Quantifying autonomous turnover. All post-assembly analyses were done using the R statistical software environment⁸³ (version 4.0.3). For fully assembled metacommunities, we simulated and stored time series of $t_{\max} = 10^4$ metacommunity samples $B_{ixt} = B_{ix}(t)$ taken in intervals of one unit time. In these metacommunity timeseries, we measured spatio-temporal turnover based on (i) compositional dissimilarity, (ii) the distribution of temporal occupancy, (iii) the number of compositional clusters detected using hierarchical clustering, and (iv) via species accumulation curves generated using sliding spatial and temporal sampling windows. Metrics were selected in order to answer specific questions, or for comparison to observed patterns. Some analyses require quantifying local species richness. This was done by setting a detection threshold of 10^{-4} biomass units, below which populations are considered absent from the community. Local source diversity, which we define in Fig. 5, is a related but different diversity measure that is more adequate for quantifying the component of a local community subject to local ecological limits to biodiversity.

Compositional dissimilarity. Spatial/temporal compositional dissimilarity was quantified using the Bray-Curtis⁴² index via the function `vegdist` in the R package “vegan”⁸⁴.

Temporal occupancy. We assessed temporal occupancy by first converting biomass into presence-absence data ($P_{ixt} = 1$ for all $B_{ixt} > 10^{-4}$, and 0 otherwise). Then, for all populations present at least once, we computed the temporal occupancy (TO_{ix}) as the proportion of the time interval of length t_{\max} during which that population was present:

$$TO_{ix} = \frac{1}{t_{\max}} \sum_t P_{ixt} \quad (3)$$

Hierarchical clustering. We assessed the degree of temporal clustering in community composition using complete linkage hierarchical clustering⁸⁵ of the Bray-Curtis dissimilarity matrix, which gives an approximate measure of the number of unstable equilibria between which the dynamical system fluctuates. We computed the number of clusters using a threshold of 25% dissimilarity, which reflects the structure visible in pairwise dissimilarity matrices (Supplementary Fig. 6a, b).

Spatio-temporal species accumulation. We studied the STR and SAR in model metacommunities using a sliding window approach, asking, for given $\Delta A \in \mathbb{N}$ and $\Delta T \in \mathbb{R}^{>0}$, how many species S^{obs} were detected on average in sets \mathcal{A} of $\Delta A = |\mathcal{A}|$ patches during any time interval \mathcal{T} of ΔT unit times length. Specifically, for a metacommunity of $N = 2^8 = 256$, the spatial windows were $\Delta A \in \{2^0, 2^1, \dots, 2^8\}$ patches, while the temporal windows were $\Delta T \in \{1, 5, 10, 50, 100, 500, 1000\}$ unit times. For each patch $x \in \{1, \dots, N\}$ the spatial sub-sample was then defined as the set \mathcal{A} consisting of the focal patch and its $\Delta A - 1$ nearest neighbours. Similarly, for each $t \in \{1, \dots, t_{\max} - \Delta T\}$ the sliding temporal window \mathcal{T} was defined as the ΔT successive recording time steps in the range t to $t + \Delta T$. The species richness observed in a given spatio-temporal sub-sample was then computed as

$$S^{\text{obs}} = \sum_i \left[\sum_{t \in \mathcal{T}} \sum_{x \in \mathcal{A}} P_{ixt} \geq 1 \right], \quad (4)$$

where the Iverson brackets $[\cdot]$ denote the indicator function ensuring species are counted only once. Finally, the average of S^{obs} for a given spatio-temporal sample size was computed in all combinations of ΔA , ΔT .

In closed systems, species accumulation in both space and time must ultimately saturate, either when the entire metacommunity or entire time series is sampled. Thus we defined the exponents z and w of the STAR as the maximum slopes of the SAR/STR on double logarithmic axes (Supplementary Fig. 13).

Reporting summary. Further information on research design is available in the Nature Research Reporting Summary linked to this article.

Data availability

Simulation data supporting a subset of the results of this study are available at <https://doi.org/10.6084/m9.figshare.14139644.v1>.

Code availability

The software used to generate these data is available at https://github.com/jacobosullivan/LVMCM_src⁸⁶.

Received: 22 June 2020; Accepted: 27 April 2021;

Published online: 15 June 2021

References

- Dornelas, M. et al. Assemblage time series reveal biodiversity change but not systematic loss. *Science* **344**, 296–299 (2014).
- Blowes, S. A. et al. The geography of biodiversity change in marine and terrestrial assemblages. *Science* **366**, 339–345 (2019).
- Kampichler, C., van Turnhout, C. A. M., Devictor, V. & van der Jeugd, H. P. Large-scale changes in community composition: determining land use and climate change signals. *PLoS One* **7** (2012).
- Newbold, T. et al. Global effects of land use on local terrestrial biodiversity. *Nature* **520**, 45–50 (2015).
- Antão, L. H. et al. Temperature-related biodiversity change across temperate marine and terrestrial systems. *Nat. Ecol. Evol.* 1–7 (2020).
- Lenoir, J. et al. Species better track climate warming in the oceans than on land. *Nat. Ecol. Evol.* 1–16 (2020).
- Lewandowska, A. M. et al. Scale dependence of temporal biodiversity change in modern and fossil marine plankton. *Global Ecology Biogeogr.* **29**, 1008–1019 (2020).
- Dornelas, M. et al. A balance of winners and losers in the anthropocene. *Ecology Lett.* **22**, 847–854 (2019).
- European Commission. Common implementation strategy for the Water Framework Directive (2000/60/EC), guidance document no. 5. *Official Journal of the European Communities* (2003).
- Magurran, A. E., Dornelas, M., Moyes, F. & Henderson, P. A. Temporal β diversity—A macroecological perspective. *Global Ecology Biogeogr.* **28**, 1949–1960 (2019).
- Law, R. & Leibold, M. A. Assembly dynamics in metacommunities. In Holyoak, M., Leibold, M. A. & Holt, R. D. (eds) *Metacommunities: Spatial Dynamics and Ecological Communities* (University of Chicago Press, 2005).
- Adler, P. B. et al. Evidence for a general species–time–area relationship. *Ecology* **86**, 2032–2039 (2005).
- White, E. P. et al. A comparison of the species–time relationship across ecosystems and taxonomic groups. *Oikos* **112**, 185–195 (2006).
- Hofbauer, J. & Sigmund, K. *Evolutionary games and population dynamics* (Cambridge University Press, 1998).
- Gilpin, M. E. Stability of feasible predator–prey systems. *Nature* **254**, 137–139 (1975).
- Smale, S. On the differential equations of species in competition. *J. Math. Biology* **3**, 5–7 (1976).
- Reichenbach, T., Mobilia, M. & Frey, E. Mobility promotes and jeopardizes biodiversity in Rock–Paper–Scissors games. *Nature* **448** (2007).
- Kerr, B., Riley, M. A., Feldman, M. W. & Bohannan, B. J. M. Local dispersal promotes biodiversity in a real-life game of rock–paper–scissors. *Nature* **418**, 171–174 (2002).
- Lotka, A. J. Elements of physical biology. *Sci. Progr. Twentieth Cent.* (1919–1933) **21**, 341–343 (1926).
- Benincà, E., Ballantine, B., Ellner, S. P. & Huisman, J. Species fluctuations sustained by a cyclic succession at the edge of chaos. *Proc. Natl. Acad. Sci.* **112**, 6389–6394 (2015).
- Remmert, H. *The Mosaic-Cycle Concept of Ecosystems* (Springer Science & Business Media, 1991).
- Leibold, M. A. & Chase, J. M. *Metacommunity Ecology* (Princeton University Press, 2018).
- O’Sullivan, J. D., Knell, R. J. & Rossberg, A. G. Metacommunity-scale biodiversity regulation and the self-organised emergence of macroecological patterns. *Ecology Lett.* **22**, 1428–1438 (2019).
- Rossberg, A. G. *Food Webs and Biodiversity: Foundations, Models, Data* (John Wiley & Sons, 2013).
- Solé, R. V. & Valls, J. On structural stability and chaos in biological systems. *J. Theor. Biol.* **155**, 87–102 (1992).
- Meszéna, G., Gyllenberg, M., Pásztor, L. & Metz, J. A. Competitive exclusion and limiting similarity: a unified theory. *Theor. Popul. Biol.* **69**, 68–87 (2006).
- Bastolla, U., Lässig, M., Manrubia, S. C. & Valleriani, A. Biodiversity in model ecosystems. I: coexistence conditions for competing species. *J. Theor. Biol.* **235**, 521–530 (2005).
- Bastolla, U. et al. The architecture of mutualistic networks minimizes competition and increases biodiversity. *Nature* **458**, 1018 (2009).
- Rohr, R. P., Saavedra, S. & Bascompte, J. On the structural stability of mutualistic systems. *Science* **345** (2014).
- Barbier, M., Arnoldi, J.-F., Bunin, G. & Loreau, M. Generic assembly patterns in complex ecological communities. *Proc. Natl. Acad. Sci.* **115**, 2156–2161 (2018).

31. Rossberg, A. G., Caskenette, A. L. & Bersier, L.-F. Structural instability of food webs and food-web models and their implications for management. In Moore, J. C., de Ruiter, P. C., McCann, K. S. & Wolters, V. (eds) *Adaptive Food Webs: Stability and Transitions of Real and Model Ecosystems*, 372–383 (Cambridge University Press, 2017).
32. Roy, F., Barbier, M., Biroli, G. & Bunin, G. Complex interactions can create persistent fluctuations in high-diversity ecosystems. *PLoS Comput. Biol.* **16** (2020).
33. Tilman, D. *Resource competition and community structure* (Princeton University Press, 1982).
34. Leibold, M. A. Similarity and local co-existence of species in regional biotas. *Evolutionary Ecology* **12**, 95–110 (1998).
35. Chase, J. M. & Leibold, M. A. *Ecological niches: linking classical and contemporary approaches* (University of Chicago Press, 2003).
36. Holt, R. D. Ecology at the mesoscale: the influence of regional processes on local communities. In Ricklefs, R. & Schluter, D. (eds.) *Species diversity in ecological communities* 77–88 (University of Chicago Press 1993).
37. Mouquet, N. & Loreau, M. Coexistence in metacommunities: the regional similarity hypothesis. *Am. Nat.* **159**, 420–426 (2002).
38. Mouquet, N. & Loreau, M. Community patterns in source-sink metacommunities. *Am. Nat.* **162**, 544–557 (2003).
39. Huffaker, C. et al. Experimental studies on predation: dispersion factors and predator-prey oscillations. *Hilgardia* **27**, 343–383 (1958).
40. Gabriel, K. R. & Sokal, R. R. A new statistical approach to geographic variation analysis. *Syst. Zoology* **18**, 259–278 (1969).
41. Matula, D. W. & Sokal, R. R. Properties of Gabriel graphs relevant to geographic variation research and the clustering of points in the plane. *Geogr. Anal.* **12**, 205–222 (1980).
42. Bray, J. R. & Curtis, J. T. An ordination of the upland forest communities of southern Wisconsin. *Ecol. Monogr.* **27**, 325–349 (1957).
43. Leibold, M. A. & Mikkelsen, G. M. Coherence, species turnover, and boundary clumping: elements of meta-community structure. *Oikos* **97**, 237–250 (2002).
44. Liataud, K., van Nes, E. H., Barbier, M., Scheffer, M. & Loreau, M. Superorganisms or loose collections of species? A unifying theory of community patterns along environmental gradients. *Ecol. Lett.* **22**, 1243–1252 (2019).
45. Arnoldi, J.-F., Barbier, M., Kelly, R., Barabás, G. & Jackson, A. L. Fitness and community feedbacks: the two axes that drive long-term invasion impacts. *Preprint at <https://doi.org/10.1101/705756v2>* (2019).
46. Rieger, H. Solvable model of a complex ecosystem with randomly interacting species. *J. Phys. A: Math. Gen.* **22**, 3447–3460 (1989).
47. Bunin, G. Ecological communities with Lotka-Volterra dynamics. *Phys. Rev. E* **95** (2017).
48. Galla, T. Dynamically evolved community size and stability of random Lotka-Volterra ecosystems. *EPL (Europhys. Lett.)* **123** (2018).
49. Hofbauer, J. Heteroclinic cycles in ecological differential equations. *Equadiff* **8** 105–116 (1994).
50. Law, R. & Morton, R. D. Alternative permanent states of ecological communities. *Ecology* **74**, 1347–1361 (1993).
51. Kessler, D. A. & Shnerb, N. M. Generalized model of island biodiversity. *Phys. Rev. E* **91** (2015).
52. Dorogovtsev, S. N., Mendes, J. F. F. & Samukhin, A. N. Giant strongly connected component of directed networks. *Phys. Rev. E* **64** (2001).
53. Ricklefs, R. E. A comprehensive framework for global patterns in biodiversity. *Ecology Letters* **7**, 1–15 (2004).
54. Coyle, J. R., Hurlbert, A. H. & White, E. P. Opposing mechanisms drive richness patterns of core and transient bird species. *The American Naturalist* **181**, E83–90 (2013).
55. Jenkins, M. F., White, E. P. & Hurlbert, A. H. The proportion of core species in a community varies with spatial scale and environmental heterogeneity. *Peer J* **6** (2018).
56. Taylor, S. J. S., Evans, B. S., White, E. P. & Hurlbert, A. H. The prevalence and impact of transient species in ecological communities. *Ecology* **99**, 1825–1835 (2018).
57. Doak, D. F. et al. The statistical inevitability of stability-diversity relationships in community ecology. *Am. Nat.* **151**, 264–276 (1998).
58. Tilman, D., Lehman, C. L. & Bristow, C. E. Diversity-stability relationships: statistical inevitability or ecological consequence? *Am. Nat.* **151**, 277–282 (1998).
59. Magurran, A. E. & Henderson, P. A. Temporal turnover and the maintenance of diversity in ecological assemblages. *Philos. Trans R. Soc. B: Biol. Sci.* **365**, 3611–3620 (2010).
60. Preston, F. W. Time and space and the variation of species. *Ecology* **41**, 612–627 (1960).
61. Adler, P. B. & Lauenroth, W. K. The power of time: spatiotemporal scaling of species diversity. *Ecol. Lett.* **6**, 749–756 (2003).
62. Shade, A., Caporaso, J. G., Handelsman, J., Knight, R. & Fierer, N. A meta-analysis of changes in bacterial and archaeal communities with time. *ISME J.* **7**, 1493–1506 (2013).
63. Drakare, S., Lennon, J. J. & Hillebrand, H. The imprint of the geographical, evolutionary and ecological context on species–area relationships. *Ecol. Lett.* **9**, 215–227 (2006).
64. Jeffries, M. J. The temporal dynamics of temporary pond macroinvertebrate communities over a 10-year period. *Hydrobiologia* **661**, 391–405 (2011).
65. Birkett, K., Lozano, S. & Rudstam, L. Long-term trends in Lake Ontario’s benthic macroinvertebrate community from 1994–2008. *Aquatic Ecosyst. Health Manag.* **18**, 76–88 (2015).
66. Mueller-Dombois, D. The mosaic theory and the spatial dynamics of natural dieback and regeneration in Pacific forests. In Remmert, H. (ed.) *The Mosaic-Cycle Concept of Ecosystems*, 46–60 (Springer, 1991).
67. White, E. P. & Gilchrist, M. A. Effects of population-level aggregation, autocorrelation, and interspecific association on the species–time relationship in two desert communities. *Evolut. Ecol. Res.* **9**, 1329–1347 (2007).
68. Burrows, M. T. et al. Ocean community warming responses explained by thermal affinities and temperature gradients. *Nat. Clim. Change* **9**, 959–963 (2019).
69. Pilotto, F. et al. Meta-analysis of multidecadal biodiversity trends in Europe. *Nat. Commun.* **11**, 1–11 (2020).
70. Vellend, M. et al. Global meta-analysis reveals no net change in local-scale plant biodiversity over time. *Proc. Natl. Acad. Sci. USA* **110**, 19456–19459 (2013).
71. Gotelli, N. J. et al. Community-level regulation of temporal trends in biodiversity. *Sci. Adv.* **3** (2017).
72. Jones, F. A. M. & Magurran, A. E. Dominance structure of assemblages is regulated over a period of rapid environmental change. *Biol. Lett.* **14** (2018).
73. Wright, J. S. Plant diversity in tropical forests: a review of mechanisms of species coexistence. *Oecologia* **130**, 1–14 (2002).
74. Curson, J., Howe, M., Webb, J., Heaver, D. & Tonhasca, A. Guidelines for the selection of biological SSSIs Part 2: Detailed guidelines for habitats and species groups. Chapter 20 invertebrates. *Guidelines for the Selection of biological SSSIs* (2019).
75. Bohan, D. A. et al. Next-generation global biomonitoring: large-scale, automated reconstruction of ecological networks. *Trends Ecol. Evol.* **32**, 477–487 (2017).
76. Martin-Platero, A. M. et al. High resolution time series reveals cohesive but short-lived communities in coastal plankton. *Nat. Commun.* **9**, 1–11 (2018).
77. Hamm, M. & Drossel, B. The concerted emergence of well-known spatial and temporal ecological patterns in an evolutionary food web model in space. *Sci. Rep.* **11**, 1–12 (2021).
78. Adler, R. J. *The Geometry of Random Fields* (SIAM, 2010).
79. Johnson, R. A. & Wichern, D. W. *Applied multivariate statistical analysis* 5 (Prentice Hall, Upper Saddle River, NJ, 2002).
80. Hindmarsh, A. C. et al. SUNDIALS: suite of nonlinear and differential/algebraic equation solvers. *ACM Trans. Math. Softw.* **31**, 363–396 (2005).
81. Gander, M. J., Halpern, L. & Nataf, F. 2. Optimized Schwarz Methods. *12th International Conference on Domain Decomposition Methods* 14 (2001).
82. King, T., Butcher, S. & Zalewski, L. Apocrita—High Performance Computing Cluster for Queen Mary University of London. (2017).
83. R Core Team. R: A Language and Environment for Statistical Computing. (R Foundation for Statistical Computing): Vienna, Austria, 2020 <https://www.R-project.org/>.
84. Oksanen, J. et al. *vegan: Community Ecology Package* (2019). R package version 2.5-6.
85. Legendre, P. & Legendre, L. *Numerical Ecology* (Elsevier, 2012), 3rd edn.
86. O’Sullivan, J. D. Intrinsic ecological dynamics drive biodiversity turnover in model metacommunities. https://github.com/jacobosullivan/LVMCM_src, <https://doi.org/10.5281/zenodo.8475> (2021).
87. Hastie, T. J. & Tibshirani, R. J. Generalized additive models *Monogr. Stat. Appl. Prob.* **64**, (1990).

Acknowledgements

We thank Lars Chittka, and Laurent Frantz for their helpful comments on earlier drafts of this paper. This work forms part of the project “Mechanisms and prediction of large-scale ecological responses to environmental change” funded by the Natural Environment Research Council (NE/T003510/1).

Author contributions

A.G.R. conceived of the study. J.D.O. and A.G.R. designed the model. J.D.O. developed the model, performed simulations, analysed the data and drafted the manuscript. J.D.O., C.D.T. and A.G.R. all interpreted model outputs in comparison with observations and contributed to manuscript writing.

Competing interests

The authors declare no competing interests.

Additional information

Supplementary information The online version contains supplementary material available at <https://doi.org/10.1038/s41467-021-23769-7>.

Correspondence and requests for materials should be addressed to J.D.O'S.

Peer review information *Nature Communication* thanks Laura Antão, Marcel Holyoak, and the other, anonymous, reviewer(s) for their contribution to the peer review of this work. Peer reviewer reports are available.

Reprints and permission information is available at <http://www.nature.com/reprints>

Publisher's note Springer Nature remains neutral with regard to jurisdictional claims in published maps and institutional affiliations.



Open Access This article is licensed under a Creative Commons Attribution 4.0 International License, which permits use, sharing, adaptation, distribution and reproduction in any medium or format, as long as you give appropriate credit to the original author(s) and the source, provide a link to the Creative Commons license, and indicate if changes were made. The images or other third party material in this article are included in the article's Creative Commons license, unless indicated otherwise in a credit line to the material. If material is not included in the article's Creative Commons license and your intended use is not permitted by statutory regulation or exceeds the permitted use, you will need to obtain permission directly from the copyright holder. To view a copy of this license, visit <http://creativecommons.org/licenses/by/4.0/>.

© The Author(s) 2021

SUPPLEMENTARY INFORMATION FILE

Distribution of interaction coefficients

In simulations described in the main text, we sampled interspecific interaction coefficients from a discrete random distribution chosen for its simplicity and relative computational efficiency. Previous work¹⁻³ has shown that macroscopic structures, including ecological limits due to the onset of structural instability, are determined by the mean and variance of the off-diagonal elements of the interaction matrix (assuming the diagonal is normalised to one), and are largely independent of finer details of the statistical distribution of entries. The discrete distribution we chose for these entries is perhaps the simplest choice for which many entries are zero (implying a sparse interaction network as typically observed in nature), that excludes non-negative terms, and is asymmetric. We expect that alternative models which preserve these basic properties, or even slightly violate them, will produce the same outcomes.

To demonstrate that this is indeed true for the model described above, we assembled metacommunities of $N = 32$ sites, spatial parameters as in main text Fig. 5, but with the entries A_{ij} sampled as products of two random variables X and Y . We sampled X from either a Beta distribution or a normal distribution, and Y as a discrete random variable with $P(Y = 1) = 0.4$ (i.e., a connectance of 0.4) and 0 otherwise. The distributions X were parameterised such that the product distribution XY preserved the expectation and variance of the discrete model used in main text Fig. 5, while keeping the matrices relatively sparse. This meant a coefficient of variation of 0.58 of the non-zero interspecific interaction terms, i.e. a fairly broad spread of values. Note that there exists no combination of parameters which preserve the mean, variance *and* connectance of the discrete model, and for which the coefficient of variance of non-zero terms is greater than zero.

As shown in Figs. 2a and b, autonomous turnover emerges in these modified metacommunity models once local communities become ecologically saturated, irrespective of the distribution from which interaction coefficients were sampled. This demonstrates that autonomous turnover arises irrespective of our choice for the distribution of interaction coefficients (Fig. 2c), and that the triggering mechanism is the same.

The simulation data used to generate Fig. 2 is publicly available⁴, while example scripts for their generation are included in the software of the LVMCM.

The variance and, to some extent, the mean of the distribution of off-diagonal elements of

A determine the local species richness at which community saturation occurs¹. To address the question whether our choice of these parameters was realistic, we note that, in real systems, the magnitude of the effective interspecific interaction coefficients A_{ij} depends, somewhat arbitrarily, on the spatial extent of the “local patches”. As we have shown in previous work⁵, effective interaction matrices for systems obtained by merging several small patches have smaller off-diagonal entries than the interaction matrices controlling the small patches themselves, and as a result these larger, merged communities can harbour a larger number of species. As such, the distribution of A_{ij} implicitly reflects the area of the local community, which we arbitrarily fixed for all sites in the model described above.

Spatial parameterization

Other than patch number N , the parameters that most impact the spatio-temporal structure of model metacommunities are the environmental correlation length ϕ , the variability of the environment σ^2 , and the dispersal length ℓ . In order to understand the role of these parameters for autonomous turnover, we fixed $N = 64$ and assembled metacommunity models with $\sigma^2, \ell \in \{1 \times 10^{-2}, 5 \times 10^{-2}, 1 \times 10^{-1}, 5 \times 10^{-1}, 1\}$, and $\phi \in \{1, 5, 10, 50, 100\}$ in all combinations and computed the resulting temporal beta diversity as the mean spatially averaged temporal BC dissimilarity observed in 10 replicates of each parameterization. Rates of autonomous turnover varied in a complex but systematic way under variation in the spatial parameterization of the model, with turnover being weakly correlated with the dispersal length and maximized for intermediate habitat heterogeneity and autocorrelation (Fig. 4). Weak abiotic heterogeneity seeds the non-uniform spatial structure of the metacommunity and therefore promotes turnover. For large enough spatial networks, dispersal limitation and competitive repulsion alone are sufficient to drive autonomous dynamics in perfectly uniform landscapes. The scan of the parameter space allowed selection a parameterization with strong autonomous turnover: $\phi = 10$, $\sigma^2 = 0.01$, $\ell = 0.5$ (peak in Fig. 4a). Using this combination of parameters we then assembled metacommunity models of $N = 8, 16, 32, 48, 64, 80, 96, 128, 160, 192, 224, 256$ patches.

To some extent, the complex roles of parameters ϕ , σ^2 , and ℓ , shown in Fig. 4, can be distilled into the effect on a single parameter: the average spatial community dissimilarity at the local neighbourhood scale. This is due to the fact that the impact of each of the parameters, which control the between-patch differences in environment and the strength of mass effects, is reflected

in the degree of spatial beta diversity within the metacommunity. To demonstrate this we used the multiple-site dissimilarity metric derived in Ref.⁶, which generates an unbiased total beta diversity metric for systems of three or more sites/time points. Since both local neighbourhood and (correspondingly) temporal turnover vary within a given metacommunity, we show the beta diversity metrics averaged over all patches.

Temporal turnover responded unimodally to local neighbourhood dissimilarity (Fig. 11) over the parameter range of Fig. 4, suggesting that spatial parameterisations that maximise β_s , either through exaggerating abiotic differences between adjacent local communities or dampening mass effects, can elevate neighbourhood diversity while simultaneously suppressing the pool of species that can actually invade.

This result makes plausible why empirical studies have detected a range of statistical associations between spatial and temporal turnover in natural ecosystems. Positive, negative, unimodal, and non-significant relationships have been reported between temporal turnover and species richness or spatial turnover^{7–12}. The unimodal response shown in Fig. 11 may help to resolve these apparent contradictions: it is not species richness or spatial dissimilarity *per se* that best predict temporal turnover, but the size of the pool of species capable of passing through biotic and abiotic filters to invade a local community.

Phase space of a generalised Lotka-Volterra community

Analytic theory² predicts a sharp transition between what has been called the Unique Fixed Point (UFP) and Multiple Attractor (MA) phases. In Fig. 7 we reproduce the phase portrait for such a system and note that our explicitly modelled metacommunities reveal a gradual transition in the MA phase space from oscillatory, to Clementsian and into Gleasonian turnover regimes. Assuming large S , the sharp transition between UFP and MA phases has been shown² to occur at species richness

$$S = \frac{2}{(1 + \gamma)^2 \text{var}(A_{ij})}, \quad (1)$$

where $\gamma = \text{corr}(A_{ij}, A_{ji})$ denotes the degree of correlation in the effects two species have on each other, measuring the symmetry of interspecific interaction strengths, and $\text{var}(A_{ij})$ is the variance in the distribution. In our model we use a random interaction matrix for which $\gamma = 0$. We sample interaction coefficients from a discrete distribution with $\text{var}(A_{ij}) = (0.25)^2$ giving

a predicted transition into the MA phase space at $S = 32$ species. Thus, while the prediction is approximate for small S communities with non-uniform intrinsic growth rates, a numerically observed threshold of around 35 species in the isolated LV model (main text Fig. 4c inset) is consistent with these analytic predictions.

Isolated LV communities

To explore the emergence of heteroclinic networks in LV models, we studied an isolated LV model with and without coupling to an implicitly modelled neighbourhood species pool. The dynamics of the model follow

$$\frac{d\mathbf{b}}{dt} = \mathbf{b} \circ (\mathbf{r} - \mathbf{A}\mathbf{b}) + \boldsymbol{\epsilon}, \quad (2)$$

where \mathbf{b} is a population biomass vector of length S , \mathbf{r} is a vector of independent random normal variables with mean 1 and variance $\sigma^2 = 0.01$ representing maximum intrinsic growth rates, \mathbf{A} is a competitive overlap matrix and the vector $\boldsymbol{\epsilon}$ represents the slow immigration of biomass corresponding to a weak propagule pressure. The elements ϵ_i are analogous to explicitly modelled immigration terms $B_{ix}D_{xy}$ of the full metacommunity model.

As in the metacommunity model, interspecific competition coefficients A_{ij} were set to 0.5 with a probability of 0.5 for $i \neq j$ and otherwise to zero, while $A_{ii} = 1$, for all i . We enforced $b_i > 0$ for all i by simulating dynamics in terms of logarithmic biomass variables. In simulating this model, we did not follow the common practice of removing species whose biomass drops below some threshold. Instead all species were retained. We consider two situations: with and without the inclusion of a weak propagule pressure $\boldsymbol{\epsilon}$.

Heteroclinic networks in the case without propagule pressure: We first demonstrate in simulations that, indeed, as predicted under certain constraints¹³, stable heteroclinic networks exist in the MA phase of model equation (1) for $\boldsymbol{\epsilon} = 0$. For this we choose $S = 300$, which, with other parameters set as described above, brings us deeply into the MA phase of the model. Simulations were initialised by setting all $B_i = 10^{-3}$ ($1 \leq i \leq S$) at $t = 0$. The system was simulated until $t = 2.1 \cdot 10^7$ and system states recorded at times $t = 2.1 \cdot 10^{j/1000}$ ($0 \leq j \leq 7000$). As illustrated in Fig. 8, while dynamics tend to become slower for larger t , no stable equilibrium or other simple attractor appears to be ever reached—as expected for a system approaching a heteroclinic network. Instead, as expected when a heteroclinic network exists, the system bounces around between un-

stable equilibria, apparently in a random fashion. Unexpected to us, however, the system appears to visit not only unstable equilibria in its transient, but occasionally also unstable periodic orbits ($t \approx 1.3 \cdot 10^4$ in Fig. 8) and perhaps more complex invariant sets ($t \approx 1.2 \cdot 10^6$ in Fig. 8).

One might wonder whether there is any tendency for dynamics to eventually come to a halt. To study this question, we calculated the number of changes in community composition (species colonisations and extinctions) between all pairs of subsequently recorded system states, where we considered a species i as “present” if $B_i > 10^{-4}$, and from this the momentary rate of change in composition on the $\ln(t)$ scale by dividing by $\ln(10^{1/1000})$. In Fig. 9 we show the time series of the centred moving average over this number for 100 subsequent pairs or recordings, and averages for non-overlapping adjacent blocks for 300 pairs. Spikes where the rate of change is particularly high correspond to brief phases of regular or irregular oscillation. We performed a median regression of the block-wise averages by a power law of the form: $(\text{rate}) \sim t^\nu$. Median regression was used to de-emphasise the spikes. For the simulation shown in Fig. 8 we found that ν did not differ significantly from zero, implying a decline of the turnover rate on the natural time axis as t^{-1} . When we repeated this analysis for 15 independent simulations (two of which failed due to numerical issues), we observed a tendency for ν to be slightly positive ($\nu = 0.054 \pm 0.020$, t-test $t = 2.67$, $p = 0.020$), perhaps because the effect of oscillatory phases on the mean turnover rate on the $\ln(t)$ -scale increases with increasing t . Overall, however, the decline of turnover rate approximately as t^{-1} was confirmed, providing evidence for the existence of an attracting heteroclinic network that the LV system equation (2) with $\epsilon = 0$ slowly approaches.

Use of logarithmic biomass variables was essential for these simulations. We found that median species biomass at the end of each run was typically around $10^{-3,500,000}$, much smaller than the smallest number representable by double precision floating point arithmetic, which is around $2 \cdot 10^{-308}$. Needless to say, these small numbers mean that the simulations with $\epsilon = 0$ are, while instructive, ecologically unrealistic.

Heteroclinic networks in the case with propagule pressure: The case $\epsilon > 0$, where dynamics move alongside the underlying heteroclinic network without ever fully approaching it, is discussed in the Main Text as it provides a useful intermediate between the explicit metacommunity model and the more tractable isolated community. In Fig. 10 we show that the transition from oscillatory to Clementsian and finally Gleasonian turnover regimes can also be observed in these isolated LV models ($\epsilon_i = \epsilon = 10^{-15}$ for all i , other parameters as above).

Local structural instability drives autonomous turnover

Species richness in competitive LV communities is intrinsically limited by the onset of ecological structural instability. Here we show analytically that for isolated communities the boundary between the UFP and MA phases² is identical to the structurally unstable limit¹.

The transition between UFP and MA phase for competitive LV models occurs² when

$$\Phi = (u - \gamma v)^2, \quad (3)$$

where $\Phi := S^*/S$ is the proportion of species persisting, i.e. the ratio between the number S^* of species that persist and the pool size S , and again $\gamma = \text{cor}(A_{ij}, A_{ji})$. The quantities u and v in equation (3) are given by

$$u = \frac{1 - \text{E}[A_{ij}]}{S^{1/2} \text{std}(A_{ij})}, \quad (4)$$

with $\text{E}[A_{ij}]$ and $\text{std}(A_{ij})$ denoting mean and standard deviation of the distribution of off-diagonal entries of \mathbf{A} , respectively, and

$$v = \frac{\Phi}{u - \gamma v}. \quad (5)$$

For $\gamma \neq 0$, equation (5) does not have a unique solution for v . The equivalent quadratic equation $\gamma v^2 - uv + \Phi = 0$ has two solutions, one of which diverges as $\gamma \rightarrow 0$; this we discard. The other solution is

$$v = \frac{u - \sqrt{u^2 - 4\gamma\Phi}}{2\gamma}, \quad (6)$$

which becomes $v = \Phi/u$ for $\gamma \rightarrow 0$, consistent with equation (5). Substitution of equation (6) into equation (3) gives

$$\Phi = \left(\frac{u - \sqrt{u^2 - 4\gamma\Phi}}{2} \right)^2, \quad (7)$$

which can be shown in a standard calculation to be equivalent to

$$\Phi = \frac{u^2}{(1 + \gamma)^2} \quad (8)$$

for $u > 0$ and $-1 < \gamma < 1$. Finally, substituting equation (4) into equation (8) gives

$$S^* = \frac{\left(1 - \mathbb{E}[A_{ij}]\right)^2}{(1 + \gamma)^2 \text{var}(A_{ij})}, \quad (9)$$

which is exactly the theoretical limit of structural instability in isolated LV communities [equation (18.3) of Ref.²⁴], thus demonstrating that UFP-MA phase boundary and the onset of structural instability perfectly coincide.

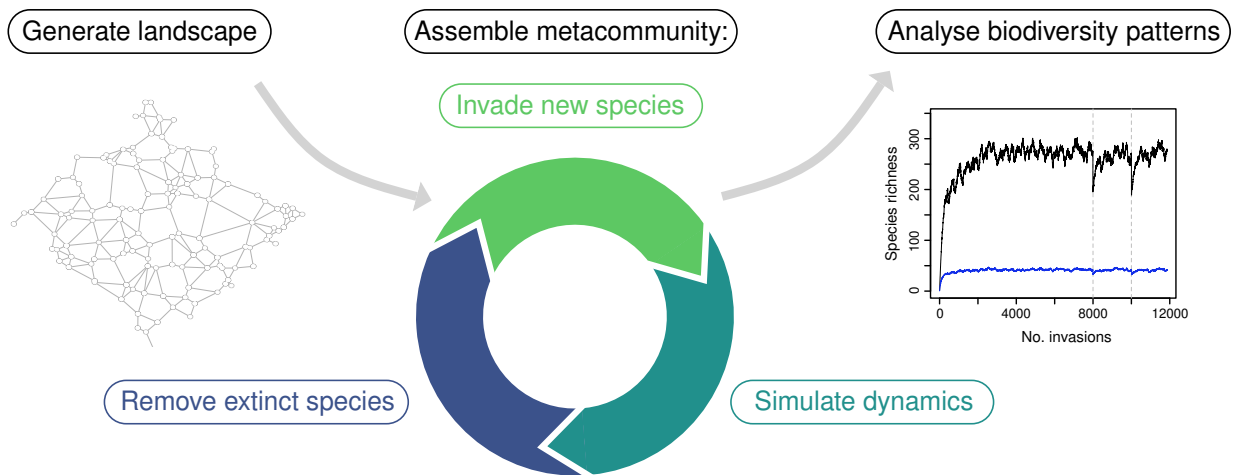
Temporal patterns in community structure

Fluctuations in local population biomasses as communities move between unstable equilibria in heteroclinic networks can span multiple orders of magnitude (red trajectories in Fig. 12a) and lead to significant temporal turnover in community composition (Fig. 12b). In contrast, the high-level properties of the assemblages remain largely unchanged. This is evident in the dampening of biomass fluctuations at metapopulation and metacommunity scales via a spatial portfolio effect^{14–16} (blue and black trajectories in Fig. 12a), but also in the robustness of species biomass distribution (Fig. 12c) and range size distribution (Fig. 12d, range sizes computed as in Ref.⁵). In this case the mean relative biomass and range size are plotted irrespective of species identity (black lines) along with the mean \pm one standard deviation (grey lines), for direct comparison with Ref.¹⁷. The relatively small standard deviations demonstrate a temporally robust distribution of metapopulation biomasses and spatial ranges, despite large fluctuations at the local scale.

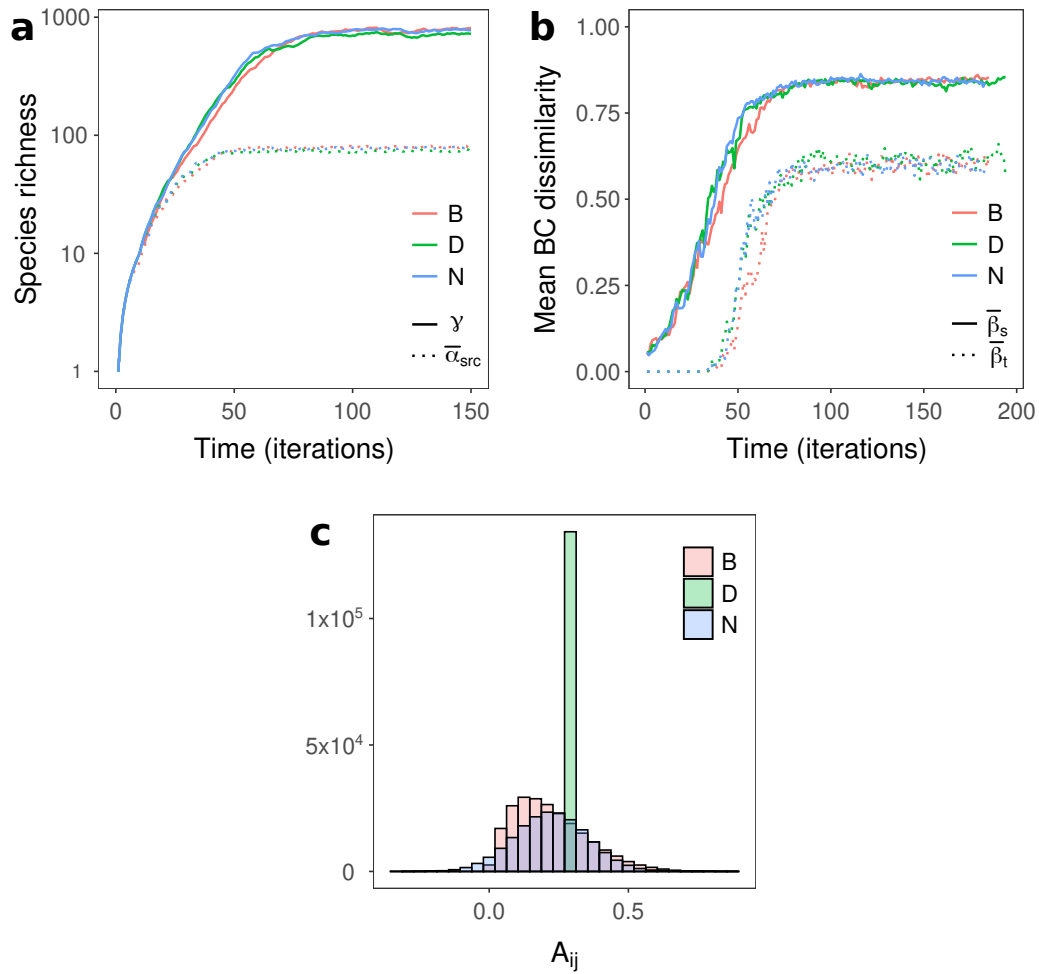
STAR in large metacommunity models

We characterised the within assemblage STAR using a moving spatio-temporal window as described in the main text and comparing the resulting SAR and STR exponents. In Fig. 13 we show the nested SAR and STR for a single metacommunity of $N = 256$. The number of species detected for large spatial or temporal windows necessarily saturates in closed systems. We therefore defined the exponents of the STAR, displayed in Fig. 6 of the main text, as the maximum slope of the SAR/STR on double logarithmic axes.

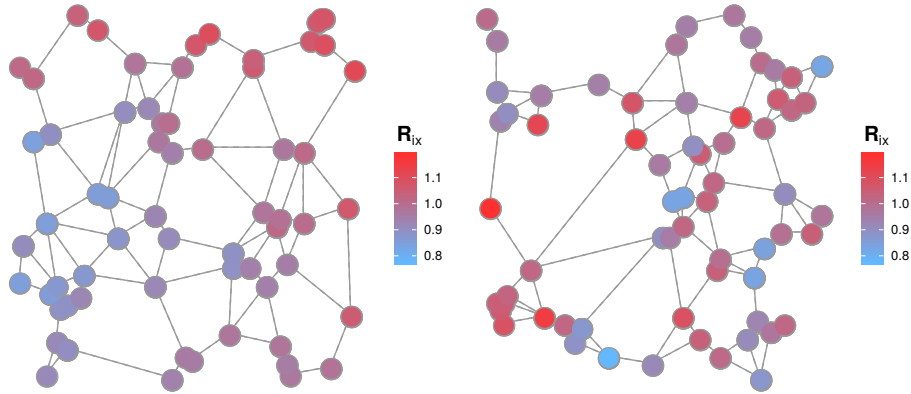
SUPPLEMENTARY FIGURES



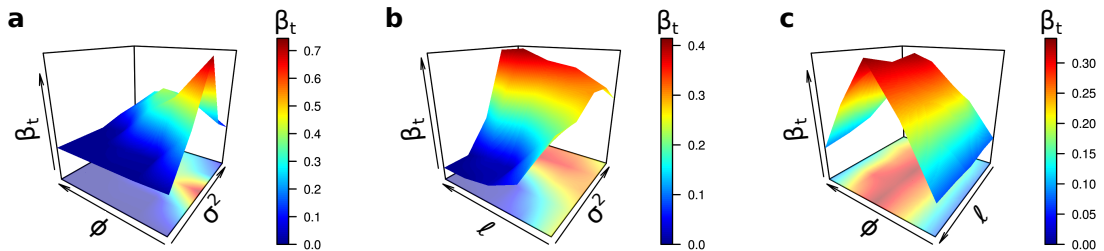
Supplementary Figure 1. **The metacommunity assembly algorithm.** First, a random planar graph is generated with spatial coordinates sampled at random and patches connected via the Gabriel² algorithm. Communities are then assembled iteratively: species are generated with intrinsic growth rates and interaction coefficients sampled from random distributions, introduced into the metacommunity at low abundance, metacommunity population-dynamics are simulated, and regionally extinct species are removed from the model before the next iteration. Eventually the metacommunity reaches both its local and regional diversity limits, the situation studied in the main text. In the inset a single metacommunity assembly process is shown; the black line represents regional species richness, the blue line average local species richness. Both are intrinsically regulated, as demonstrated by the effect of random removals of species (dashed lines) and subsequent re-assembly: local richness is barely affected and regional richness returns to the approximate same level. Inset adapted from Ref.⁵. See text for detailed description.



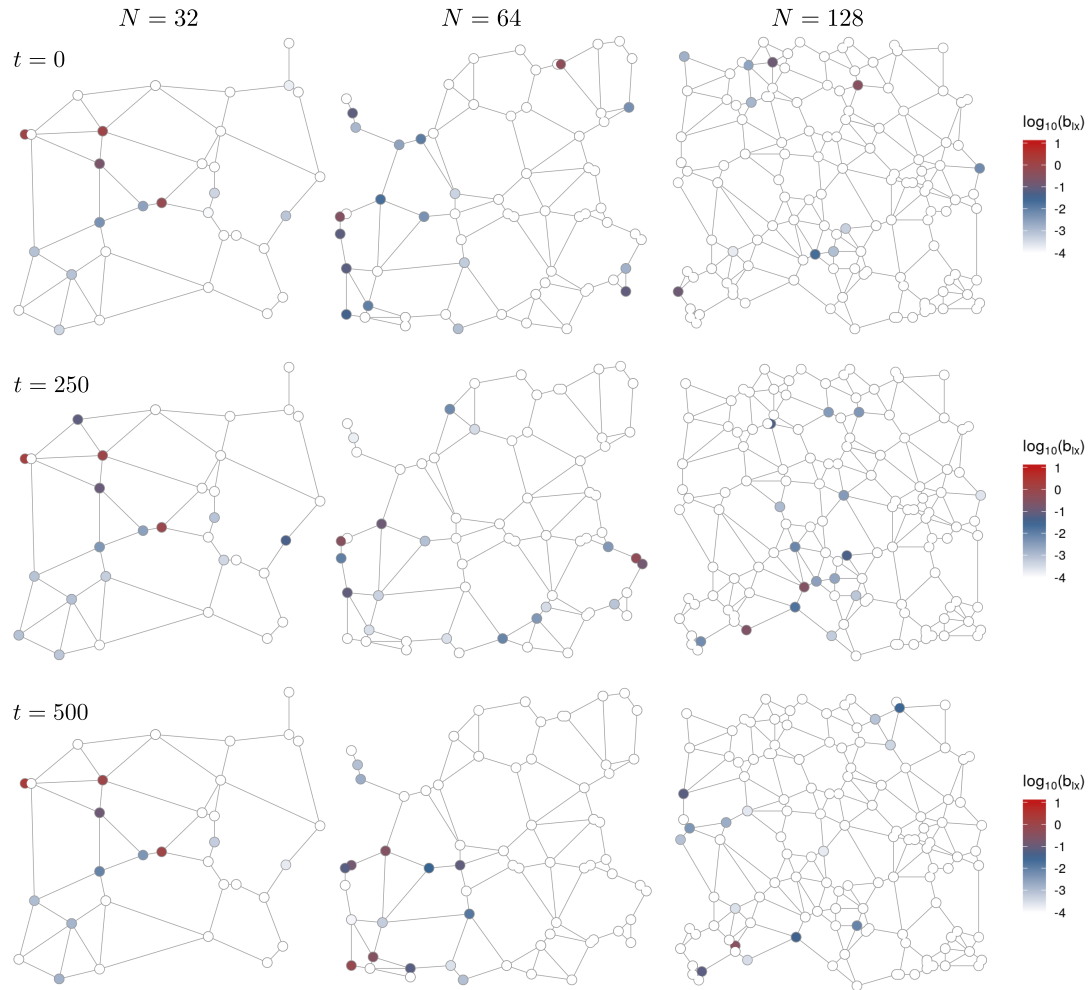
Supplementary Figure 2. **Autonomous turnover in different random matrix metacommunities.** **a:** Metacommunity assemblies with A_{ij} sampled from a Beta distribution with connectance 0.4 (B); a discrete distribution with $P(A_{ij} = 0.3) = 0.3$ as in main text Fig. 5 (D); and a normal distribution with connectance 0.4 (N). In all cases, the mean and variance of the fundamental distributions were identical. Shown are the regional diversity γ and the mean local richness of source populations $\bar{\alpha}_{src}$ since this is the community component directly subject to ecological limits. Here, in each iteration of the assembly model (regional invasion event), $0.1S + 1$ species were introduced and a total 10^4 invasions were simulated. **b:** As shown in main text Fig. 5, autonomous turnover sets in once local communities become saturated with respect to species richness. **c:** The realised distributions in *non-zero* interaction coefficients A_{ij} after metacommunity assembly. For visual clarity $A_{ij} = 0$, representing 71.4%, 61.1% and 61.4% of interspecific interaction coefficients for the D, B and N distributions respectively, have been removed.



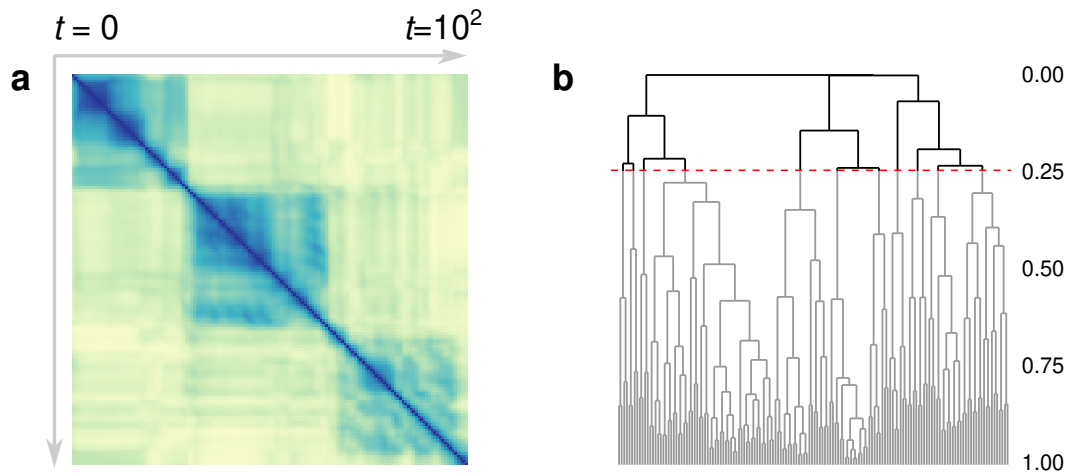
Supplementary Figure 3. **Spatially autocorrelated growth rate distributions.** Intrinsic growth rates are sampled from spatially autocorrelated random fields of autocorrelation length ϕ and variance σ^2 . Two example distributions are shown, both for $N = 64$, $\sigma^2 = 0.01$, with $\phi = 10$ (left) and $\phi = 1$ (right). See Materials and Methods for details.



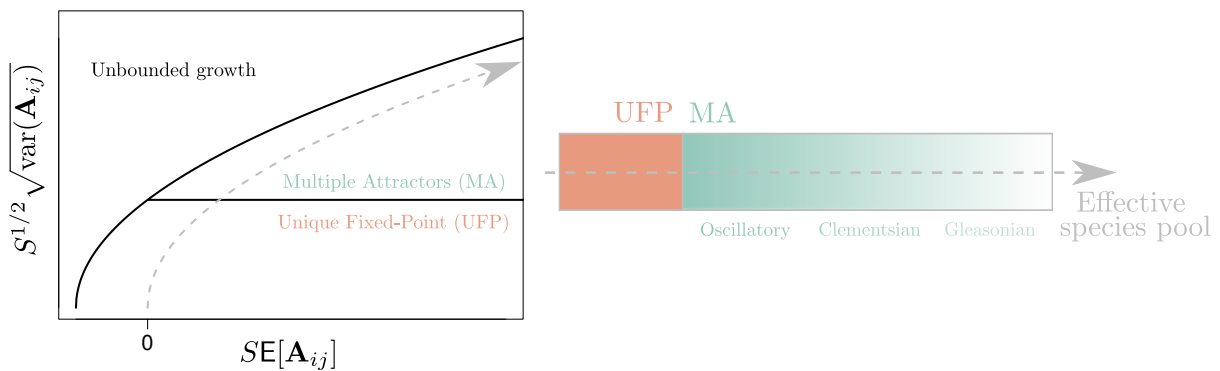
Supplementary Figure 4. **Temporal turnover throughout the spatial parameter space.** Temporal β -diversity β_t was computed as the mean BC dissimilarity between time points in a time series of 1000 unit times, observed in metacommunities of $N = 64$ patches. Correlation length ϕ was varied in the range 1 to 100, environmental variability σ^2 and dispersal length ℓ in the range 10^{-2} to 1, with each parameter combination replicated 10 times. The values of ϕ , σ^2 and ℓ were each plotted on logarithmic axes. In **a** we fixed ℓ at 0.5; in **b** ϕ at 10; and in **c** σ^2 at 1.0. See Supplementary discussion for details.



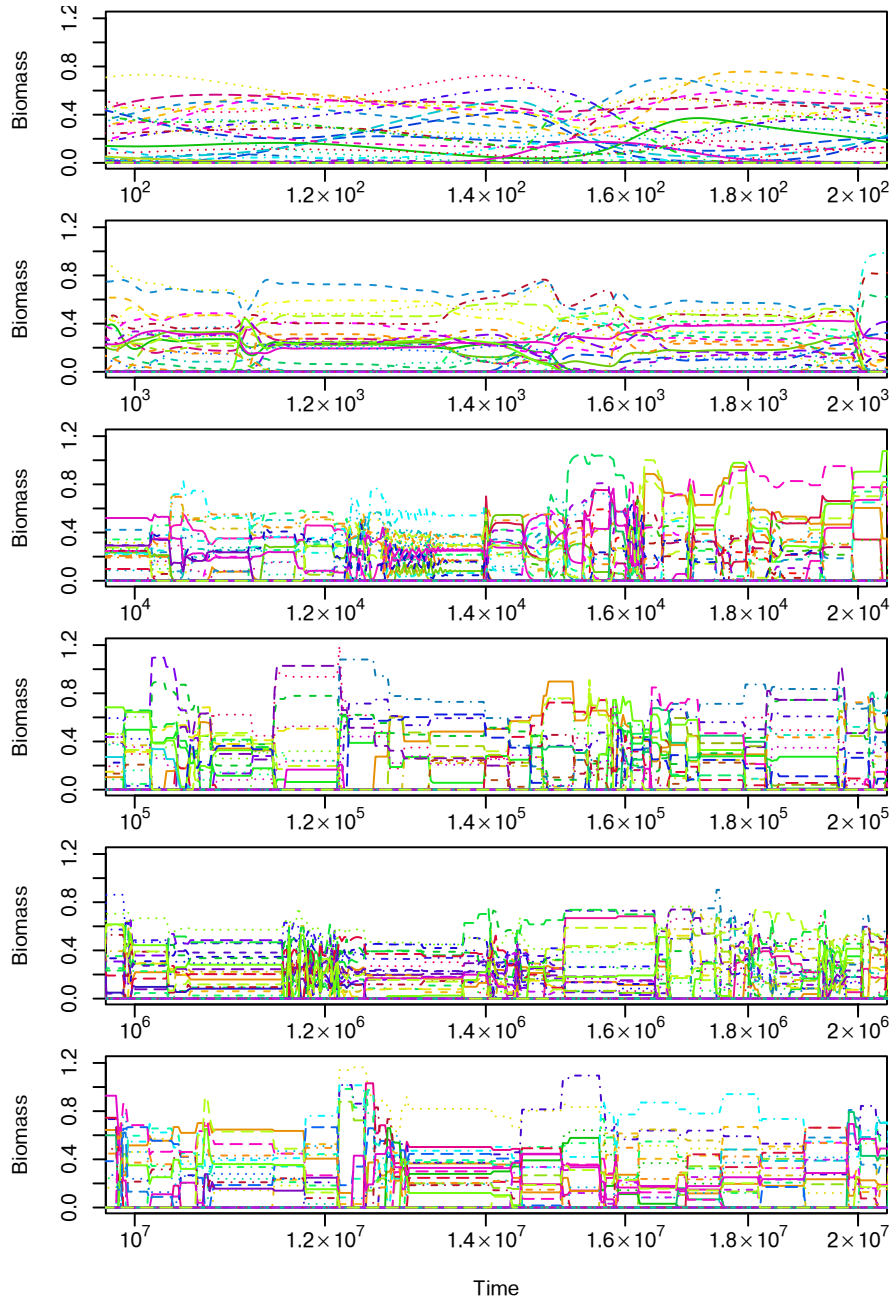
Supplementary Figure 5. **Autonomous metapopulation dynamics in large metacommunity models.** In species rich metacommunities of $N > 8$ patches, local biomasses autonomously fluctuate and the variability of those fluctuations increases with metacommunity size. Here we show the instantaneous biomass distributions for a single species in metacommunities of $N = 32, 64$ and 128 , at three time points in logarithmic biomass units. For $N = 32$, autonomous fluctuations are largely restricted to the outer extremes of the species' distribution, while the core range (left of network) remains largely static. For $N = 64$, some patches or regions may be permanently occupied by the focal species, however even in this core range biomass can fluctuate by orders of magnitude. With the emergence of Gleasonian turnover in the high N limit no or few patches are permanently occupied and local community composition is no longer well characterised by the core-transient distinction^{17?}, which decomposes local communities into populations that are present almost all the time, and those observed only rarely. Hence, for $N = 128$ no obvious core range exists. Note that spatial networks are not shown to scale, the area of the model landscape is $\approx N$ in all cases. $A_{ij} = 0.5$ with probability 0.5, $\phi = 10$, $\sigma^2 = 0.01$, $\ell = 0.5$. See Main Text for details.



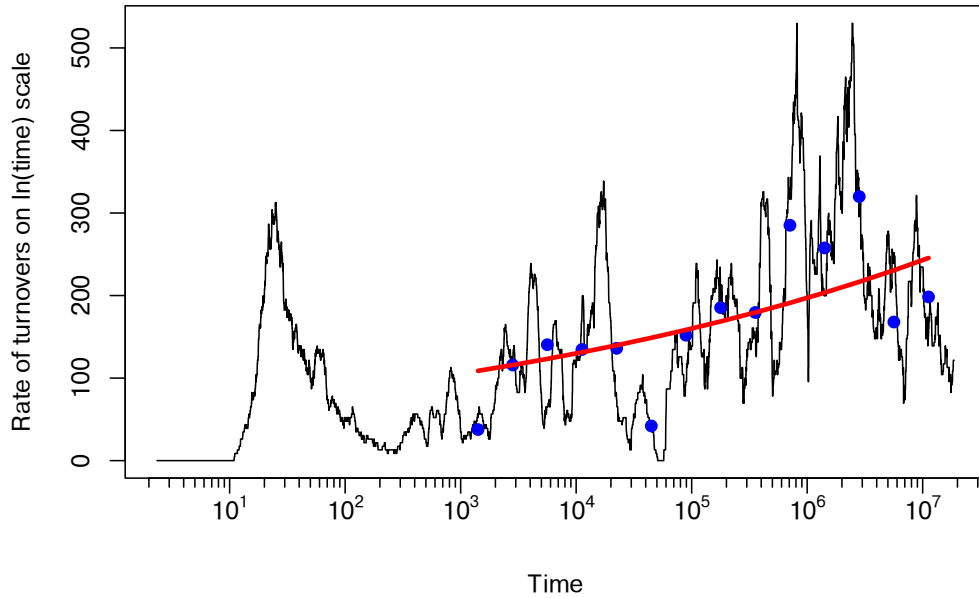
Supplementary Figure 6. **The number of compositional clusters in a community time-series analysed using hierarchical clustering.** **a:** Temporal clustering in local community composition represented by the block structure of the BC dissimilarity matrix ($N = 64$, 200 unit times shown). **b:** Using hierarchical cluster analysis we approximately quantified the number of clusters in community state using a dissimilarity threshold of 25% (red dashed line).



Supplementary Figure 7. **The sharp transition between UFP and MA phases.** Reproduction of the phase diagram derived by Bunin² showing the emergence of MA as the size S of the species pool increases. In our case, the first and second moments of the distribution in A_{ij} were fixed. Community state in phase space therefore follows a square root function with increasing S , as indicated by the dashed line. (The “Unbounded growth” phase is hence not relevant for our study.) In spatially explicit metacommunity models we observe the emergence of autonomous turnover which transitions from oscillations to Clementsian and finally Gleasonian turnover. See Supplementary discussion for details.

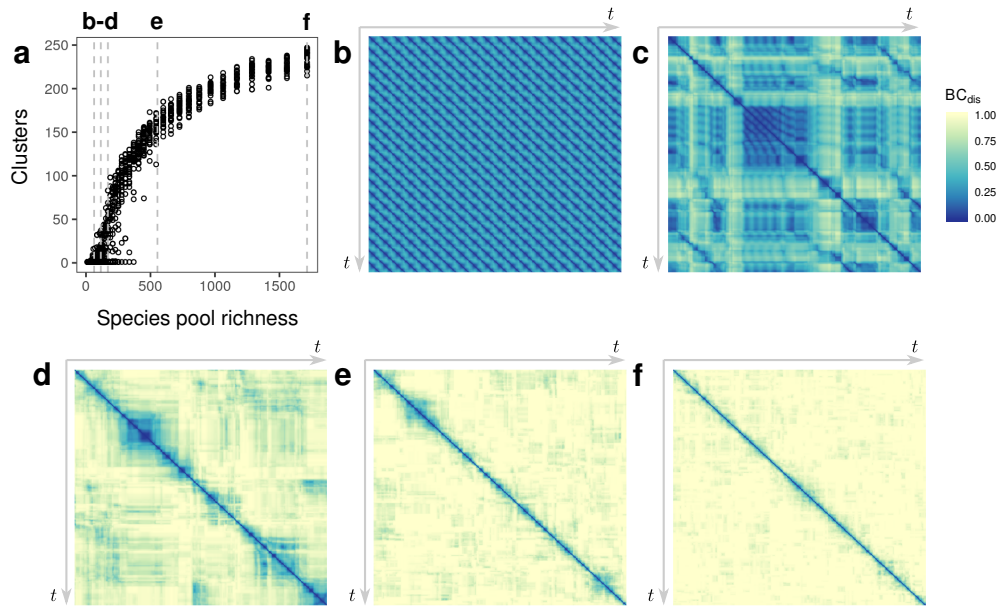


Supplementary Figure 8. **Episodes in the approach of an isolated LV community model to a heteroclinic network.** The biomasses of different species are represented by lines of different colours and style. At any moment in time, all but a few of the $S = 300$ species in the system have biomasses close to zero. With increasing simulation times t the intervals between the switches in system state, corresponding to transitions from the vicinity of one unstable equilibrium to the next, become longer, while the duration of these transitions remains of the order of magnitude of 10 time units, leading to increasingly sharper transitions on the logarithmic time scale. See Supplementary discussion for details.

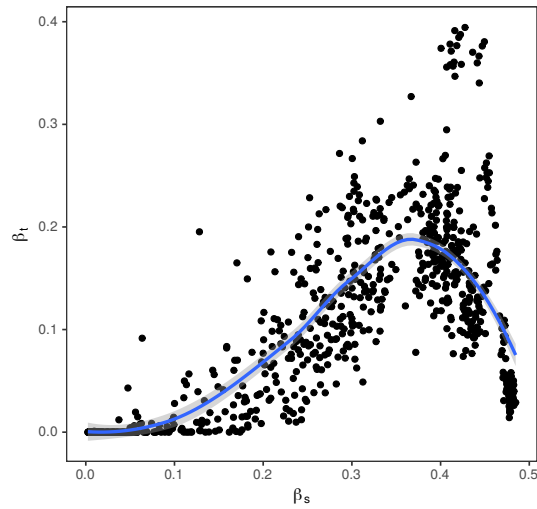


Supplementary Figure 9. **Rate of change in community composition for the simulation shown in Fig. 8.**

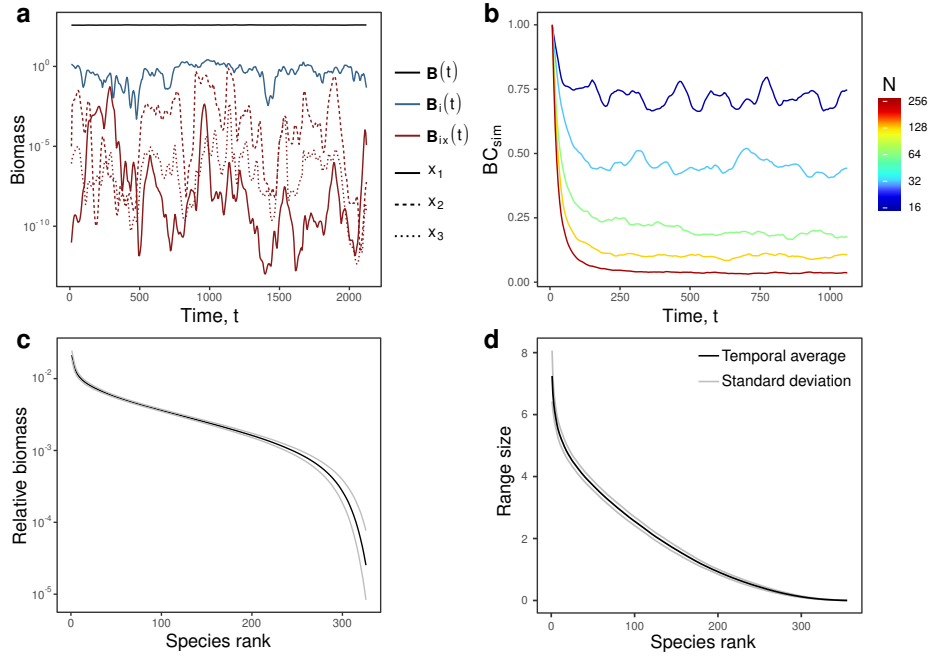
The black line is the moving average over 100 subsequent recordings, blue dots represent averages over non-overlapping adjacent blocks of 300 recordings for $t \geq 1000$, and the red line a median nonlinear regression of the dots by a power-law (rate) $\sim t^\nu$ ($\nu = 0.091 \pm 0.062$, not significantly different from zero). See Supplementary discussion for details.



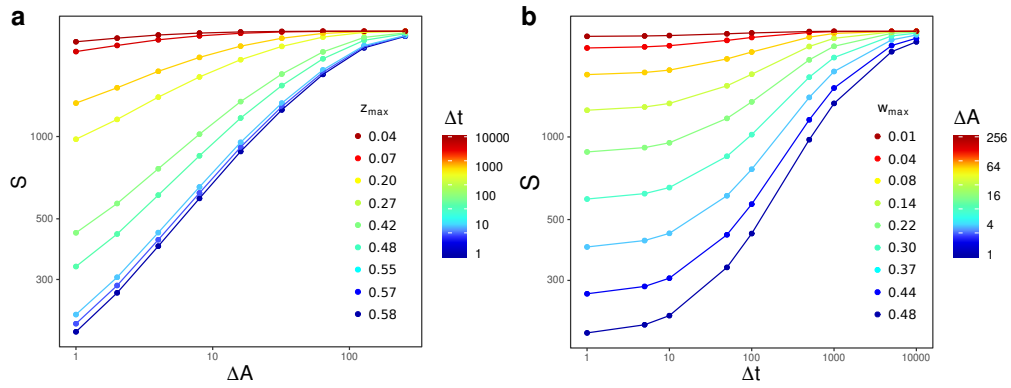
Supplementary Figure 10. **Autonomous turnover in isolated LV communities.** **a:** The number of compositional clusters detected as a function of the size of the pool of potential invaders for a propagule pressure, ϵ , of 10^{-15} biomass units per unit time. **b-f:** Heatmaps of the pairwise Bray-Curtis dissimilarity for the corresponding time-series (over 10^4 unit times) showing a clear transition from oscillatory to Clementsian turnover and finally to Gleasonian turnover. Dashed lines in **a** show the size of the species pool for which each community time series was generated. $A_{ij} = 0.5$ with probability 0.5, $\sigma^2 = 0.01$. The parameters ϕ and ℓ are not defined for the isolated LV models. See Supplementary discussion for details.



Supplementary Figure 11. **Unimodal relationship between spatial and temporal turnover.** Temporal beta diversity, computed during 1000 unit times, plotted against the spatial beta diversity of the local neighbourhood. The number of patches in a local neighbourhood depends on the patch degree, which varies. We therefore use a beta-diversity metric⁶ (based on BC dissimilarity) that normalises by the number of sites/time-points included in the sub-sample. Both β_t and β_s are averages over the metacommunity. The blue line and shaded area represent a locally weighted regression (LOESS smoothing) and 95% C.I.. Parameters N , ϕ , σ^2 and ℓ as in Fig. 4. See Supplementary discussion for details.



Supplementary Figure 12. **Temporally robust community structure a:** We highlight the scale dependence of autonomous population dynamics by showing the biomass of three random local populations of the same species (B_{ix} , red), of the metapopulation of which they form a part ($B_i = \sum_x B_{ix}$, blue) and finally of the entire metacommunity ($B = \sum_i \sum_x B_{ix}$), black). **b:** Autonomous turnover can be substantial. Here we show the decay of spatially averaged BC *similarity* from an arbitrary initial composition in metacommunities of $N = 16, 32, 64, 128,$ and 256 patches. For large metacommunities undergoing autonomous Gleasonian turnover, the percentage of permanent populations, and hence the temporal BC similarity can drop to zero. **c:** Metacommunity scale relative rank abundance curve, plotted with species ‘identity’ disregarded. The black curve represents the mean biomass observed at a given rank, while grey curves represent the mean \pm one standard deviation. This figure highlights the temporally invariant diversity structure at the metacommunity scale. **d:** The temporally averaged rank range size curve, plotted as in c. $A_{ij} = 0.5$ with probability 0.5, $\phi = 10$, $\sigma^2 = 0.01$, $\ell = 0.5$. $N = 64$ for **a**, **c** and **d**. See Supplementary discussion for details.



Supplementary Figure 13. **The Species-Time-Area-Relation.** The nested SAR (a) and STR (b) generated using a sliding window approach for a single metacommunity model of $N = 256$. Metacommunity models are closed systems and as such, both the SAR and STR saturate for the large sub-samples. Therefore, we defined the exponents of the STAR by the maximum slopes observed on double logarithmic axes. $A_{ij} = 0.5$ with probability 0.5, $\phi = 10$, $\sigma^2 = 0.01$, $\ell = 0.5$. See Supplementary discussion for details.

-
- [1] Rossberg, A. G. *Food Webs and Biodiversity: Foundations, Models, Data* (John Wiley & Sons, 2013).
- [2] Bunin, G. Ecological communities with Lotka-Volterra dynamics. *Physical Review E* **95** (2017).
- [3] Barbier, M., Arnoldi, J.-F., Bunin, G. & Loreau, M. Generic assembly patterns in complex ecological communities. *Proceedings of the National Academy of Sciences* **115**, 2156–2161 (2018).
- [4] O’Sullivan, J., Terry, C. & Rossberg, A. G. Intrinsic ecological dynamics drive biodiversity turnover in model metacommunities: Supporting data <https://doi.org/10.6084/m9.figshare.14139644.v1> (2021).
- [5] O’Sullivan, J. D., Knell, R. J. & Rossberg, A. G. Metacommunity-scale biodiversity regulation and the self-organised emergence of macroecological patterns. *Ecology Letters* **22**, 1428–1438 (2019).
- [6] Legendre, P. & De Cáceres, M. Beta diversity as the variance of community data: dissimilarity coefficients and partitioning. *Ecology letters* **16**, 951–963 (2013).
- [7] White, E. P. *et al.* A comparison of the species-time relationship across ecosystems and taxonomic groups. *Oikos* **112**, 185–195 (2006).
- [8] Shurin, J. B. *et al.* Diversity–stability relationship varies with latitude in zooplankton. *Ecology Letters* **10**, 127–134 (2007).
- [9] Ptacnik, R. *et al.* Diversity predicts stability and resource use efficiency in natural phytoplankton communities. *Proceedings of the National Academy of Sciences* **105**, 5134–5138 (2008).
- [10] Ptacnik, R., Andersen, T., Brettum, P., Lepistö, L. & Willén, E. Regional species pools control community saturation in lake phytoplankton. *Proceedings of the Royal Society B: Biological Sciences* **277**, 3755–3764 (2010).
- [11] Korhonen, J. J., Soininen, J. & Hillebrand, H. A quantitative analysis of temporal turnover in aquatic species assemblages across ecosystems. *Ecology* **91**, 508–517 (2010).
- [12] Stegen, J. C. *et al.* Stochastic and deterministic drivers of spatial and temporal turnover in breeding bird communities. *Global Ecology and Biogeography* **22**, 202–212 (2013).
- [13] Hofbauer, J. Heteroclinic cycles in ecological differential equations. *Equadiff* **8** 105–116 (1994).
- [14] Doak, D. F. *et al.* The statistical inevitability of stability-diversity relationships in community ecology. *The American Naturalist* **151**, 264–276 (1998).
- [15] Tilman, D., Lehman, C. L. & Bristow, C. E. Diversity-stability relationships: statistical inevitability or ecological consequence? *The American Naturalist* **151**, 277–282 (1998).

- [16] Yachi, S. & Loreau, M. Biodiversity and ecosystem productivity in a fluctuating environment: the insurance hypothesis. *Proceedings of the National Academy of Sciences* **96**, 1463–1468 (1999).
- [17] Magurran, A. E. & Henderson, P. A. Temporal turnover and the maintenance of diversity in ecological assemblages. *Philosophical Transactions of the Royal Society B: Biological Sciences* **365**, 3611–3620 (2010).